



A STUDY OF CLOUDS IN THAILAND USING GROUND AND SATELLITE BASED DATA



A Thesis Submitted in Partial Fulfillment of the Requirements

for Doctor of Philosophy PHYSICS

Department of PHYSICS

Graduate School, Silpakorn University

Academic Year 2021

Copyright of Silpakorn University

การศึกษาเมฆจากข้อมูลภาคพื้นดินและข้อมูลดาวเทียมในประเทศไทย



วิทยานิพนธ์นี้เป็นส่วนหนึ่งของการศึกษาตามหลักสูตรปรัชญาดุษฎีบัณฑิต

สาขาวิชาฟิสิกส์ แบบ 1.1 ปรัชญาดุษฎีบัณฑิต

ภาควิชาฟิสิกส์

บัณฑิตวิทยาลัย มหาวิทยาลัยศิลปากร

ปีการศึกษา 2564

ลิขสิทธิ์ของมหาวิทยาลัยศิลปากร

A STUDY OF CLOUDS IN THAILAND USING GROUND AND SATELLITE BASED
DATA



A Thesis Submitted in Partial Fulfillment of the Requirements
for Doctor of Philosophy PHYSICS
Department of PHYSICS
Graduate School, Silpakorn University
Academic Year 2021
Copyright of Silpakorn University

Title A study of clouds in Thailand using ground and satellite based data
 By MISS Sahussa PEENGAM
 Field of Study PHYSICS
 Advisor Professor Dr. Serm Janjai

Graduate School Silpakorn University in Partial Fulfillment of the Requirements
 for the Doctor of Philosophy

.....Dean of graduate school
 (Associate Professor Jurairat Nunthanid, Ph.D.)

Approved by

.....Chair person
 (Associate Professor Dr. Wilawan Kamharn)

.....Advisor
 (Professor Dr. Serm Janjai)

.....Committee
 (Assistant Professor Dr. Itsara Masiri)

.....Committee
 (Assistant Professor Dr. Sumaman Buntoung)

.....Committee
 (Assistant Professor Dr. Korntip Tohsing)

61306802 : Major PHYSICS

Keyword : Physical properties of cloud, Cloud optical thickness, Cloud effective radius

MISS SAHUSSA PEENGAM : A STUDY OF CLOUDS IN THAILAND USING GROUND AND SATELLITE BASED DATA THESIS ADVISOR : PROFESSOR DR. SERM JANJAI

This research can be divided into three parts. The first part is to investigate the optical thickness of low cloud at Nakhon Pathom station (13.82°N, 100.04°E), Thailand during 2019-2020. A method for determining the physical properties of cloud from a spectroradiometer with a radiative transfer model (LibRadtran) was carried out. According to the method, cloud optical thickness (COT) for ultraviolet, visible and near-infrared radiation were determined under an overcast sky. It was found that the COT in the UV and visible wavelengths are approximately similar and the COT increases in the near-infrared wavelengths. These observation results correspond to the theory.

The second part of the research is a mapping of COT and cloud effective radius (r_e) over Thailand using satellite data. In this work, the COT and r_e have been derived using a radiative transfer model (SBDART) together with data from Himawari-8 satellite during 2016-2020. The maps of monthly average values of COT and r_e were generated, and the characteristics of COT and r_e were analyzed. The maps show the seasonal variations of COT and r_e .

In the final part, maps of total cloud amount over Thailand using satellite data were generated. In this study, a model relating cloud cover obtained from ground-based measurement (Skyviews, model PSV-100) and cloud index retrieved from MTSAT-1R satellite data at four stations in Thailand during 2009-2016 was developed. This model was used to estimate cloud cover at four sites. The result of the model validation in terms of root mean square difference (RMSD) and mean bias difference (MBD) were found to be 12.9% and 3.5%, respectively. After the validation, the model was used to estimate cloud amount over Thailand and the results are shown as monthly and yearly maps.



ACKNOWLEDGEMENTS

In my studies for the degree of Doctor of Philosophy (Physics), it would not be accomplished well without the help of the following people.

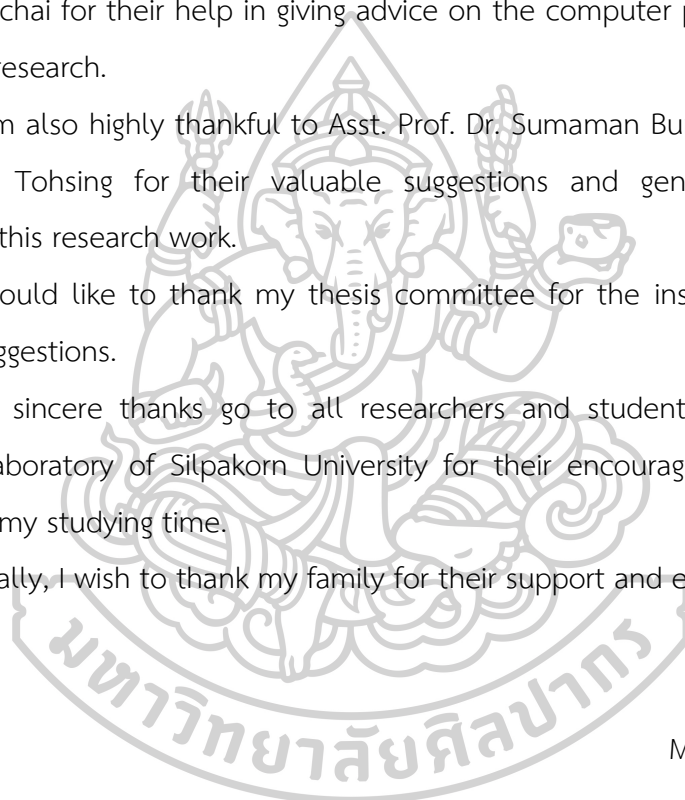
I would like to express my sincere thanks to my advisor, Professor Dr. Serm Janjai for his helpful guidance, enthusiastic encouragement, and support throughout this study. I am deeply indebted to Asst. Prof. Dr. Itsara Masiri and Asst. Prof. Dr. Somjet Pattarapanitchai for their help in giving advice on the computer program for calculating data in my research.

I am also highly thankful to Asst. Prof. Dr. Sumaman Buntoung and Asst. Prof. Dr. Korntip Tohsing for their valuable suggestions and generous encouragement throughout this research work.

I would like to thank my thesis committee for the insightful comments and valuable suggestions.

My sincere thanks go to all researchers and students in the Solar Energy Research Laboratory of Silpakorn University for their encouragement, and friendship throughout my studying time.

Finally, I wish to thank my family for their support and entire care.



MISS Sahussa PEENGAM

TABLE OF CONTENTS

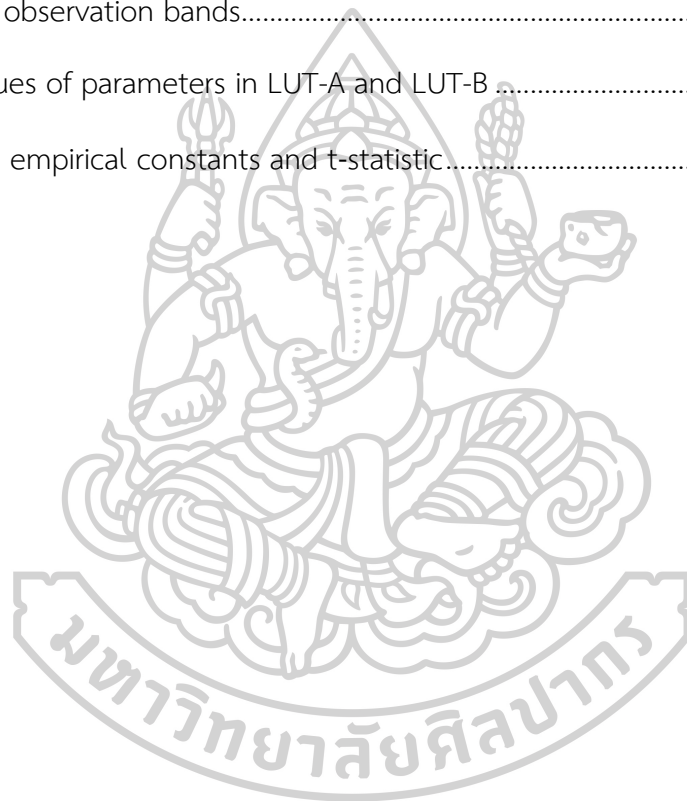
	Page
ABSTRACT	D
ACKNOWLEDGEMENTS	F
TABLE OF CONTENTS	G
LIST OF TABLES	I
LIST OF FIGURES	J
CHAPTER 1 INTRODUCTION	1
1.1 Rationale of the study	1
1.2 Objectives	2
1.3 Scope of the Research	2
1.4 Organization of this thesis	3
CHAPTER 2 THEORY AND LITERATURE REVIEW	4
2.1 Clouds	4
2.2 Cloud formation processes	4
2.3 Classification of cloud	5
2.4 Physical properties of cloud	10
2.5 Literature reviews	12
CHAPTER 3 METHODS, RESULTS AND DISCUSSION	16
3.1 An investigation of optical thickness of clouds at Nakhon Pathom station	16
3.2 COT and r_e mapping over Thailand by using satellite data	25
3.3 Cloud cover from satellite data over Thailand	38
CHAPTER 4 CONCLUSIONS	49

Appendix	50
Comparison of solar spectrum from measurements and that from radiative transfer model under overcast sky condition.....	50
REFERENCES	58
VITA.....	63



LIST OF TABLES

	Page
Table 1 LWC values (Kampe, 1950; Hess et al., 1998).....	10
Table 2 Cloud effective radius (Hess et al., 1998; Stephens, 1994).....	11
Table 3 The parameters used in the model	20
Table 4 AHI observation bands.....	26
Table 5 Values of parameters in LUT-A and LUT-B	30
Table 6 The empirical constants and t-statistic.....	43



LIST OF FIGURES

	Page
Figure 1 The climate system (from website: https://mpimet.mpg.de/en/communication/multimedia/figures/climate-system).....	4
Figure 2 Conditionally unstable air (Ahrens, 2014).....	5
Figure 3 Cumulus humilis (Photographed by Frank Le Blancq (World Meteorological Organization, 2022)).....	6
Figure 4 Cumulus mediocris (Photographed by Frank Le Blancq (World Meteorological Organization, 2022)).....	6
Figure 5 Cumulus congestus (Photographed by Chi Yung Lau (World Meteorological Organization, 2022)).....	7
Figure 6 Cirrus cloud (Photographed by Sahussa Peengam, the author of this thesis) .	8
Figure 7 Altcumulus cloud (Photographed by Stefan Käme (World Meteorological Organization, 2022)).....	8
Figure 8 Nimbostratus cloud (Photographed by Jarmo Koistinen (World Meteorological Organization, 2022)).....	8
Figure 9 Cloud classification according to the height (World Meteorological Organization, 2022).....	9
Figure 10 Nakhon Pathom station.....	17
Figure 11 The diagram shows the working principle of the radiative transfer model..	17
Figure 12 The instruments used in this work (a) sky camera, (b) sunphotometer, (c).	18
Figure 13 Examples of sky conditions under (a) Clear sky (b) Partly cloudy sky and (c) Overcast sky.....	18
Figure 14 Cloud optical thickness determination process.....	21

Figure 15 Examples of spectral solar irradiance under overcast sky from the spectroradiometer at 10.30 a.m. local time of different days in September 2019.....	22
Figure 16 COT in low-level cloud	23
Figure 17 Satellite data from (a) band number 2, (b) band number 7 and (c) band number 13.....	27
Figure 18 Correlation between reflectivity and radiance from band 2.....	28
Figure 19 Correlation between brightness temperature and radiance from band 7 ...	28
Figure 20 Correlation between brightness temperature and radiance from band 13 .	29
Figure 21 Diagram showing the algorithm to determine COT and r_e adapted from Nakajima et al. (1995)	31
Figure 22 Mapping of COT and r_e values obtained from satellite data on 1 January 2017 at 8.30 a.m. (a) satellite imagery in band number 2 (Visible wavelength), (b) COT mapping and (c) r_e mapping.	34
Figure 23 Monthly average cloud optical thickness over Thailand.....	36
Figure 24 Monthly average cloud effective radius over Thailand	37
Figure 25 A map of Thailand showing the locations of the study sites and the pictorial view of the skyviews used in this work. A, B, C and D indicate the Northern, Northeastern, Central and the Southern regions, respectively.	39
Figure 26 The comparison between monthly average cloud cover from the skyviews algorithm and visual observation.....	40
Figure 27 An example of a navigated image and the locations of the ground-based stations.....	42
Figure 28 The relation between monthly average cloud cover from the sky images (\bar{C}) and monthly average cloud index (\bar{n}) from the satellite data.....	43
Figure 29 Comparison between cloud cover from the proposed model and that from the sky images at the four stations.....	44

Figure 30 Monthly average cloud cover over Thailand (color code: 0 represents clear sky and 10 is completely overcast)..... 46

Figure 31 Long-term yearly average cloud cover over Thailand..... 47



CHAPTER 1

INTRODUCTION

1.1 Rationale of the study

The world is covered by clouds approximately 60%-70% (Quante, 2004). Clouds contribute for our lives and environment in both direct and indirect ways (Lamb & Verlinde, 2011). Clouds are important to the atmospheric system and part of water cycle. High and thin clouds can attenuate outgoing longwave radiation, resulting in the greenhouse effect. Low and thick clouds can reflect solar radiation (Cotton & Anthes, 1992). These can affect the Earth's energy balance.

To calculate solar radiation at the ground under cloudy sky, satellite or physical approach can be used. However, this approach is complicated (Tohsing et al., 2021). An alternative to this approach is employed the optical thickness of cloud. Cloud optical thickness (COT) is a parameter of the cloud optical properties. COT depends on the physical properties such as cloud thickness, liquid or ice water content, effective radius, cloud types, and area of cloud formation (Aebi et al., 2020; World Meteorological Organization, 1988). Recently, many scientists attempted to find methods to determine the physical properties of clouds including COT in several areas. Most of them used broadband ground-based data to estimate the properties of clouds. For example, Serrano et al. (2015) used broadband pyranometers and UV radiometers to estimate COT at Valencia, Spain, and Aebi et al. (2020) and Leontieva et al. (1994) used broadband pyranometers to obtain COT, and r_e at Payern, Switzerland. There are also some researches using spectroradiometers (Wilson et al., 2018) to calculate COT at West Antarctic. From these recent researches, most of them studied in Europe and America, where clouds occur as ice clouds. As Thailand is located in the tropical zone, clouds are generally liquid water clouds. In addition, the study of cloud properties in Thailand is limited. Therefore, part of this study aims

to estimate COT at a site in the tropical zone by using a spectroradiometer. Furthermore, the wavelength dependent of COT will be also investigated.

In order to obtain the cloud properties over broader areas, a satellite approach is an alternative method. For example, Nakajima and King (1995) used satellites to determine COT and r_e from reflected solar radiation. This method can estimate the COT and r_e over the west coast of California. In Thailand, the research work on mapping of physical cloud properties (COT and r_e) from satellite data has not yet been published. Therefore, the purposes of this research are to estimate the COT and r_e over Thailand using satellite data and to generate the maps of COT and r_e .

Apart from COT and r_e , total cloud amount in the sky is also an important property of cloud. It is a variable that affects the solar radiation incident the Earth's surface. Generally, cloud amount is visually observed at meteorological stations around the world. The method of measurements based on human eye estimates, resulting in inaccuracies and not covering all areas. Therefore, in this research, we developed a method for estimating cloud cover using satellite data over Thailand.

1.2 Objectives

The specific objectives of this study are as follows.

- 1) To determine COT from ground-based measurements at Nakhon Pathom, Thailand
- 2) To determine cloud properties from satellite data over Thailand
- 3) To determine cloud amount from satellite data over Thailand

1.3 Scope of the Research

This research will study the COT using the data obtained from the spectroradiometer installed at Nakhon Pathom station, Department of Physics, Faculty of Science, Silpakorn University. COT and r_e mapping over Thailand from satellite data will be carried out, and finally total cloud amount mapping from satellite data over Thailand will be undertaken.

1.4 Organization of this thesis

This thesis consists of 4 chapters. The first chapter is the rationale of the study. The second chapter is the theory and literature review. The third chapter presents COT at Nakhon Pathom, COT and r_e mapping over Thailand, and the total cloud amount mapping over Thailand. Finally, the conclusion will be presented in chapter 4.



CHAPTER 2

THEORY AND LITERATURE REVIEW

2.1 Clouds

Cloud is a hydrometeor consisting of small particles of liquid water or ice, or of both, suspended in the atmosphere and above the earth's surface (World Meteorological Organization, 1988). There are many different types of clouds, depending on the weather conditions in that area. Clouds are an important for weather forecasts. Also, it is very important in the water cycle because clouds can be condensed to become the rain, help to drive entire climate system (Figure 1).

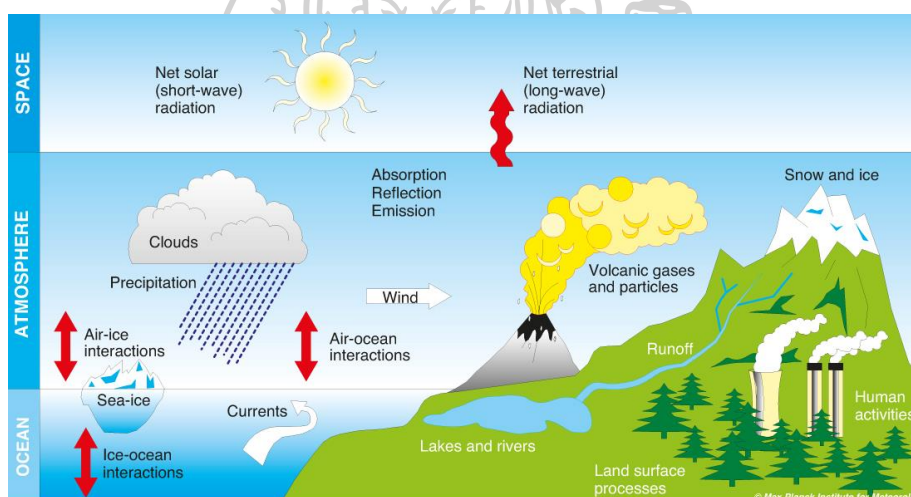


Figure 1 The climate system (from website: <https://mpimet.mpg.de/en/communication/multimedia/figures/climate-system>)

2.2 Cloud formation processes

Generally, the cloud formation process involves the convection of air parcels and cooling. Whereas the disintegration of clouds is the sinking of the air parcel and the rise in temperature which depends on the stability of the air. If the air temperature is equal to dew-point temperature, the relative humidity is 100 percent. This air parcel will condense. The height at which condensation occurs is called level

of condensation. Water vapor changes to water, which is called “cloud droplet”. This is the starting point for cloud formation. We often notice that the bottom of the clouds is semi-linear and call this area "cloud base", in which the condensation will contain aerosols in the air such as dust, salt spray, pollen, etc., acting as core particles (condensation nuclei) in condensation.

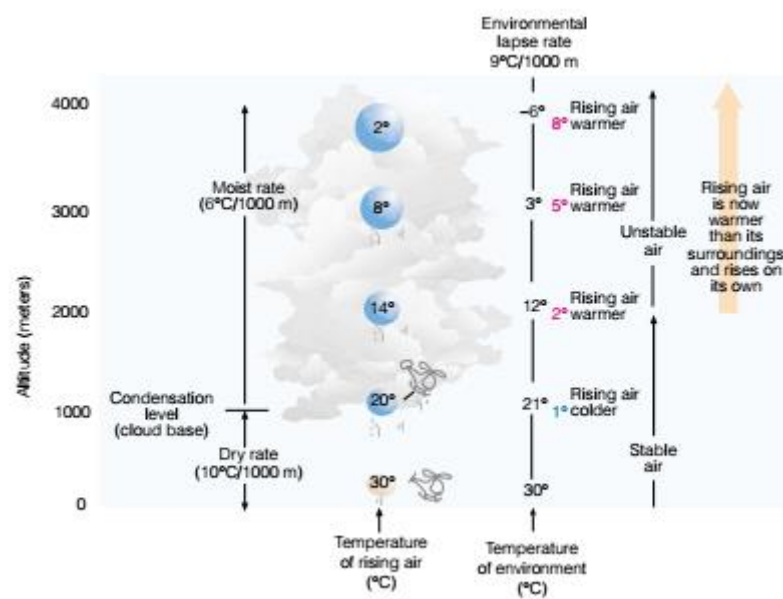


Figure 2 Conditionally unstable air (Ahrens, 2014)

2.3 Classification of cloud

Clouds are classified according to several criteria as follows.

2.3.1 Types of clouds according to their appearance and shape

- Stratiform cloud

Stratiform clouds are horizontally layered clouds and spread into wide regions, taking on an appearance of a sheet. Examples of stratiform clouds include nimbostratus, stratus, altostratus, cirrostratus, and cirrus.

- Cumuliform cloud

There is a vertical growth of convective clouds called "cumulus clouds", a word that comes from the Latin word, divided into 3 sub-types.

- Humilis
- Mediocris
- Congestus



Figure 3 Cumulus humilis (Photographed by Frank Le Blancq
(World Meteorological Organization, 2022))



Figure 4 Cumulus mediocris (Photographed by Frank Le Blancq
(World Meteorological Organization, 2022))



Figure 5 Cumulus congestus (Photographed by Chi Yung Lau
(World Meteorological Organization, 2022))

Examples of cumuliform clouds include cumulus, cumulus congestus, and cumulonimbus.

2.3.2 Types of clouds according to the height of clouds

- High cloud

High clouds are clouds with a level of the cloud base is more than 6,000 meters and consist of ice crystals, such as Cirrus (Cano et al., 1986), Cirrostratus (Cs) and Cirrocumulus (Cc) clouds.

- Middle cloud

Middle clouds are clouds with a level of the cloud base is between 2,000 meters and 7,000 meters. It consists of water droplets. But if the temperature is low enough, the clouds will consist of ice crystals, such as Altostratus (As) and Altocumulus (Ac) clouds.

- Low Cloud

Low clouds are clouds with a level of the cloud base is lower than 2,000 meters, such as Stratus (St), Stratocumulus (Sc), and Nimbostratus (Ns) clouds.



Figure 6 Cirrus cloud (Photographed by Sahussa Peengam, the author of this thesis)

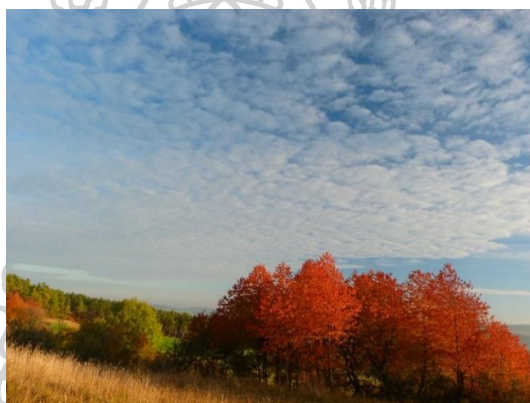


Figure 7 Altocumulus cloud (Photographed by Stefan Käme
(World Meteorological Organization, 2022))



Figure 8 Nimbostratus cloud (Photographed by Jarmo Koistinen
(World Meteorological Organization, 2022))

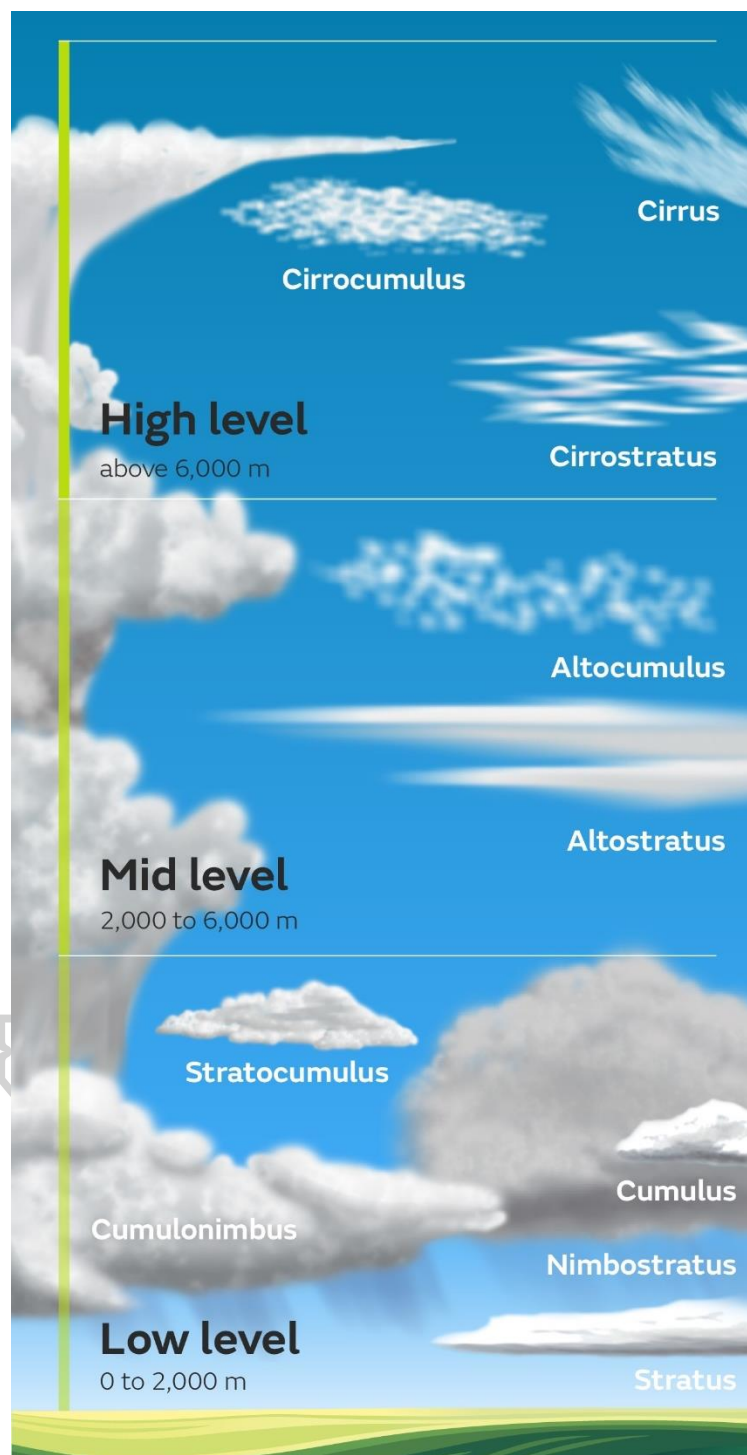


Figure 9 Cloud classification according to the height (World Meteorological Organization, 2022)

2.4 Physical properties of cloud

2.4.1 Cloud liquid water content

Cloud liquid water content (LWC) is a measure of the total liquid water contained in a cloud in a vertical column of the atmosphere, not including snow or ice. LWC is a highly variable measure and depends on the type of clouds presenting at a given location, given in units mass of water per volume of air (g/m^3) or per mass of air (g/kg) (Remote Sensing Systems, 2022). Values of LWC are shown in Table 1.

Table 1 LWC values (Kampe, 1950; Hess et al., 1998)

Cloud type	LWC (g/m^3)
Cirrus	0.026
Stratus	0.2-0.3
Cumulus	0.26
Altostratus	0.20

2.4.2 Cloud liquid water path

Cloud Liquid water path (LWP) is a measure of the weight of the liquid water droplets in the atmosphere above a unit surface area on the earth, given in units of kg/m^2 or g/m^2 (CLIMATE DATA GUIDE NCAR, 2020). The liquid water path can be approximately retrieved from passive and active remote sensing such as microwave radiometer instruments. LWP is a parameter that allows to understand the physical processes of clouds (condensation, evaporation, and the occurrence of rain) and helps understand a radiative transfer in clouds. Typically, mean of a stratocumulus has an LWP of approximately $20\text{-}80 \text{ g/m}^2$. It can be obtained from the equation: (American Meteorological Society, 2012).

$$\text{LWP} = \int \rho_{\text{air}} r_L dz \quad (1)$$

where LWP is liquid water path

ρ_{air} is the density of the (wet) air

r_L is the liquid water mixing ratio.

2.4.3 Cloud effective radius

Cloud effective radius (r_e) is a measure for the mean size in a particle population in clouds. The extinction of radiation by a particle is governed by the cross-section area of the particle (Liou, 1992; McFarquhar & Heymsfield, 1998; Wyser, 1998) r_e can be defined as:

$$r_e = \frac{\int_0^{\infty} r \pi r^2 n(r) dr}{\int_0^{\infty} \pi r^2 n(r) dr} \quad (2)$$

where r_e is the cloud effective radius

r is the radius of particles

$n(r)dr$ is the number of particles per unit volume with radius between r and $r + dr$.

Cloud effective radius depends on types of cloud which can be shown in Table 2.

Table 2 Cloud effective radius (Hess et al., 1998; Stephens, 1994)

Cloud type	r_e (μm)
Cirrus	34.3-91.7
Stratus	7.3
Cumulus	5.7
Altostratus	10.0

2.4.4 Cloud optical thickness

Cloud optical thickness (COT) is a measure of attenuation of the light passing through the atmosphere due to the scattering and absorption by cloud droplets. COT is relatively independent of wavelength throughout the visible spectrum but rises rapidly in the infrared due to absorption by water. COT usually follows using the relationship (Barnard & Long, 2004) :

$$\text{COT} = \frac{3\text{LWP}}{2r_e} \quad (3)$$

where COT is cloud optical thickness

LWP is cloud liquid water content

r_e is cloud effective radius.

2.5 Literature reviews

From the importance of cloud properties especially cloud optical thickness and cloud effective radius and to better understand the role of clouds in the Earth's climate system, scientists need to know values of these parameters. Following studies are examples of the work.

There are several works determining properties of clouds from ground-based measurements. Leontieva et al. (1994) used ground-based measurements of incoming solar irradiance and cloud observations during a 26-year period (1965–1990) at Bergen, Norway in conjunction with a comprehensive radiation model to infer the cloud optical thickness under completely overcast conditions. Month-to-month and year-to-year (April through October) statistics of the cloud optical depth and observed cloud forms are presented. The values of cloud optical thickness for high clouds are less than 5 and cloud effective radius is 7 μm .

Marshak et al. (2004) studied a new method for retrieving cloud optical depth from ground-based measurements of zenith radiance in the red (RED) and near-infrared (NIR) spectral regions. The proposed retrieval method is applied to Cimel (sunphotometer) measurements at the Atmospheric Radiation Measurements (ARM)

site in Oklahoma. The preliminary results look very promising both theoretically and from measurements.

Nauss et al. (2011) used a new technique relying on Simple Approximations for cLOUDy Media (SLALOM) for the retrieval of cloud optical and microphysical parameters from optical satellite data during daytime. The technique was based on simple highly accurate approximations of the asymptotic solutions of the radiative transfer theory which have already been implemented in the forward radiative transfer model cloud. The comparison of SLALOM with both exact radiative transfer computations and the NASA MODIS cloud property product showed a very good agreement.

Wilson et al. (2018) used a shortwave spectroradiometer deployed on the West Antarctic Ice Sheet (WAIS) as part of the U.S. Department of Energy Atmospheric Radiation Measurement (ARM) program ARM West Antarctic Radiation Experiment (AWARE). This instrument measured spectral irradiance covering the wavelength range 350–2,200 nm. Using micro-pulse lidar data to identify the thermodynamic phase of stratiform clouds cooperated with radiative transfer algorithm to retrieve optical depth and effective droplet (or particle) size for single-phase liquid water and ice water clouds. This work found that, before the melt event, most liquid cloud effective droplet radius was consistent with pristine polar maritime clouds with the value of 13.5 μm . Most ice clouds sampled occurred before the melt event has the optical depth of 4 and cloud effective particle size of 19 μm .

Aebi et al. (2020) used a pyranometer measuring broadband solar radiation and radiative transfer models (RTMs) in order to estimate the following cloud optical properties: cloud optical thickness (COT), cloud single scattering albedo (SSA_c) and effective droplet radius (r_e) during 2013–2017, at the Baseline Surface Radiation Network (BSRN) station in Payerne, Switzerland. It was found that COT are between 12 and 92 with a geometric mean and standard deviation of 33.8 and 1.7, respectively. The comparison of these COT values from model and from empirical equation (Barnard and Long, 2004) results in a mean difference of -1.2 ± 2.7 . The values of COT were also compared with MODIS satellite data. There is a larger mean

difference of around 18. The estimated r_e for stratus and altostratus clouds are between 2 and 20 μm .

In Thailand, Nimnuan et al. (2017) derived the effective droplet radius and optical depth of liquid water clouds using spectroradiometer at ultraviolet wavelength (440 nm.), aircraft observations and an adiabatic model of cloud liquid water at Omkoi (17.80°N, 98.43°E), Thailand. Monthly averages of cloud optical depth are highest in April (54.5), which is the month with the lowest average cloud effective radius (4.2 μm), both occurring before the start of the rainy season and at the end of the high contamination period.

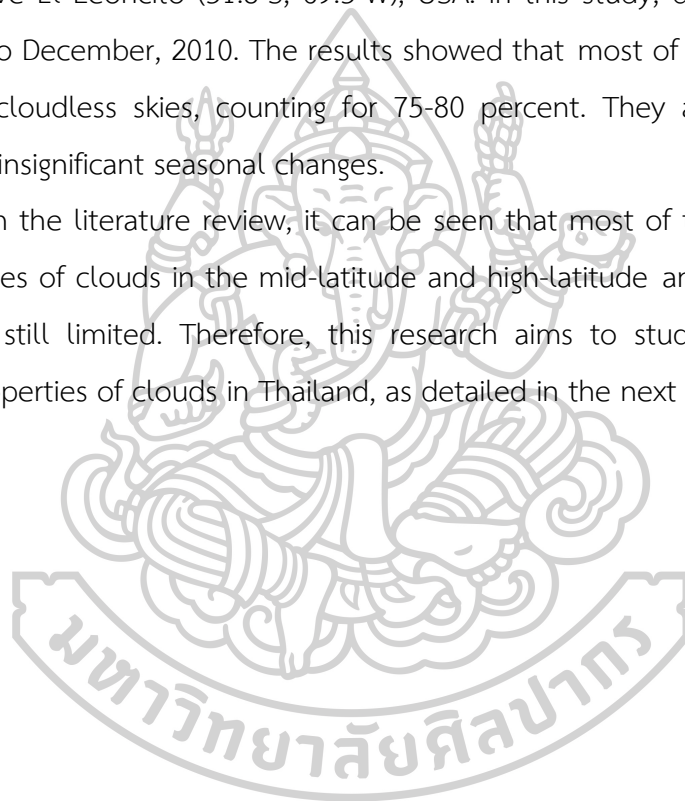
For determination of cloud properties over a wider region, there is only the work of Nakajima et al. (1990) who presented the method for determining the optical thickness and effective particle radius of stratiform cloud layers from reflected solar radiation measurements of satellite data. A detailed study is presented showing that the cloud optical thickness (COT) and effective particle radius (r_e) of water clouds can be determined solely from reflection function measurements at 0.75 and 2.16 μm , providing $\text{COT} \geq 4$ and $r_e \geq 6 \mu\text{m}$. For optically thin clouds, the retrieval becomes ambiguous, resulting in two possible solutions for the effective radius and optical thickness. Adding a third channel near 1.65 μm does not improve the situation noticeably, whereas the addition of a channel near 3.70 μm reduces the ambiguity in deriving the effective radius. The effective radius determined by the above procedure corresponds to the droplet radius at some optical depth within the cloud layer. For clouds having $\text{COT} \geq 8$, the effective radius determined using the 0.75 and 2.16 μm channels can be regarded as 85%–95% of the radius at cloud top, which corresponds in turn to an optical depth 20%–40% of the total optical thickness of the cloud layer.

There are some studies on fraction of cloud in the sky. Huo and Lu (2009) quantified clouds from sky images taken from the All-sky Imager system (ASIs-I) of the Institute of Atmospheric Physics in Beijing, China. They used radiation transmission models to determine the limits of cloudiness. The ratio of the solar spectrum at wavelengths 450 nm (blue) and 650 nm (red) was used to separate cloudless and cloudy skies. From this research, it was found that the ratio of the

solar spectrum under cloudless sky condition was higher than that under partly cloudy and overcast sky conditions. This is because air molecules can scatter blue light better than red light, while clouds can scatter these two colors equally. It also suggests that the amount of particulate matter in the atmosphere affects cloud amount. Because the aerosols in the atmosphere makes the change of the solar spectrum ratio.

Martinis et al. (2013) proposed a method for calculating cloud cover from sky images above El Leoncito (31.8°S, 69.3°W), USA. In this study, data were used from May, 2006 to December, 2010. The results showed that most of the sky at this site is under the cloudless skies, counting for 75-80 percent. They also found that the clouds had insignificant seasonal changes.

From the literature review, it can be seen that most of the research studied the properties of clouds in the mid-latitude and high-latitude and the studies in the tropics are still limited. Therefore, this research aims to study the quantity and physical properties of clouds in Thailand, as detailed in the next chapter.



CHAPTER 3

METHODS, RESULTS AND DISCUSSION

In this research, cloud properties were investigated in Thailand. The work can be subdivided into three parts. The first part is to estimate cloud optical thickness based on ground-based spectral radiation at Nakhon Pathom station. In the second work, mapping of cloud properties from the Himawari-8 satellite data was carried out over Thailand. For the final part, cloud cover from the satellite data was also undertaken. The details are presented as follows.

3.1 An investigation of optical thickness of clouds at Nakhon Pathom station

We investigated cloud optical thickness (COT) on overcast days at Nakhon Pathom station (Figure 10), by using solar spectrum from ground-based measurements and a radiative transfer model. The algorithm used in this work to obtain the COT is presented in Figure 11. Firstly, the exact atmospheric parameters such as aerosol optical depth (AOD), aerosol single scattering albedo (SSA), precipitable water (W), total column ozone (O_3), and varying cloud properties such as COT and r_e are used as inputs in the radiative transfer model. The model will give output as spectral solar irradiance. This irradiance will be compared with the measured spectral irradiance. The COT that gives the best closest values will be selected.



Figure 10 Nakhon Pathom station

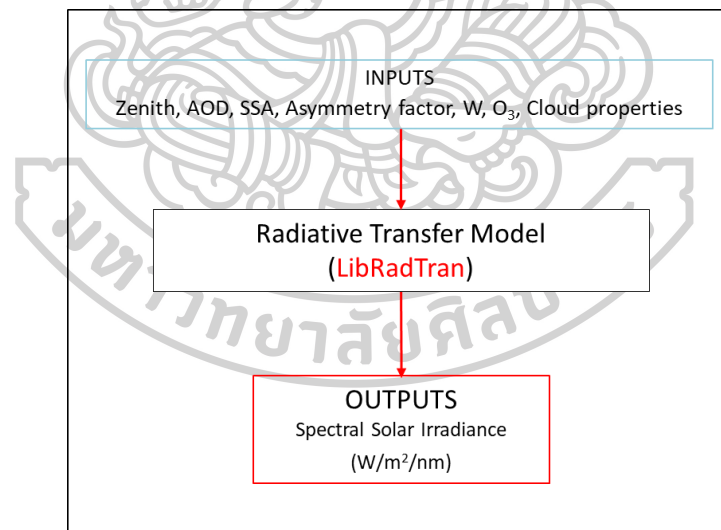


Figure 11 The diagram shows the working principle of the radiative transfer model.

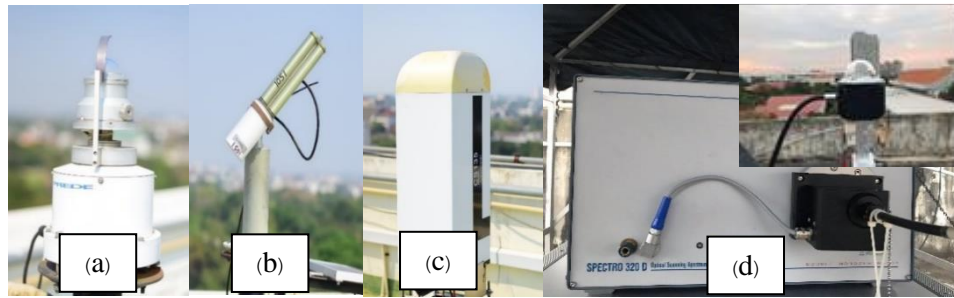


Figure 12 The instruments used in this work (a) sky camera, (b) sunphotometer, (c) ceilometer and (d) spectroradiometer

3.1.1 The instruments and data

All ground-based instruments used in this work were installed at Silpakorn University (13.82°N, 100.04°E), Nakhon Pathom, Thailand (Figure 10) and we call it Nakhon Pathom station. The data from these instruments encompass a period: 2019-2020. The details are as follows.

In this work, we selected only the data under overcast sky. In order to identify the sky conditions, we used a sky camera (PREDE, model PSV-100) (Figure 12(a)) that captured the images of the sky. Examples of images from the sky camera for clear sky, partly cloudy and overcast sky are shown in Figure 13. In this work, we used data only for the sky condition being as in Figure 13(c).

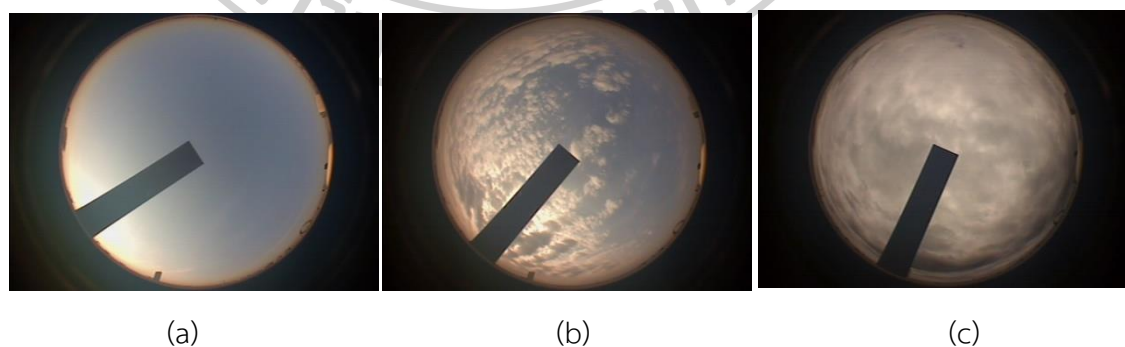


Figure 13 Examples of sky conditions under (a) Clear sky (b) Partly cloudy sky and (c) Overcast sky.

Parameters used in the radiative transfer model include solar zenith angle (θ_z), aerosol optical depth (AOD), single scattering albedo (SSA), asymmetry factor of aerosols, surface albedo, precipitable water (W), total ozone column (O_3) and cloud properties (Table 3). The hourly AOD, SSA, asymmetry factor, surface albedo and W were derived from a sunphotometer (Cimel, model: CE318, see Figure 13(b)). This instrument is a part of AERONET (Aerosol RObotic NETwork) and the data are available on <https://aeronet.gsfc.nasa.gov/>.

Total ozone column was retrieved from OMI/AURA satellite and the data are on the website: <https://avdc.gsfc.nasa.gov/pub/data/satellite/Aura/OMI/V03/L2OVP/>. The total ozone column retrieved from this database is daily basis. We will use this value constantly during the day.

For the cloud properties, the cloud base height (CBH) was measured by a ceilometer (Campbell Scientific, model: CS135) (Figure 13(c)). This ceilometer uses the NIR laser at wavelength of 905 nm which can observe four layers of the cloud base height up to 10 km. The liquid water content (LWC) is assumed to be constant following Table 1 (Chapter 2), which depends on the type of cloud. The liquid water path (LWP) and cloud effective radius (r_e) are obtained from the recent research on effective radius of cloud at Omkoi, Chiang Mai, Thailand (Nimnuan et al., 2017).

The spectral solar irradiance used to compare with the output of the radiative transfer model is measured by a spectroradiometer (Instrument System, model: SP-320D, see Figure 13(d)). The wavelength ranges of the measurements are 220-2,400 nm. The resolution for the wavelength range of 220-1,700 nm is 1 nm and for the wavelength range of 1,700-2,400 nm is 20 nm.

Table 3 The parameters used in the model

Input data	Source of data
Solar zenith angle	Calculation (Iqbal, 1983)
AOD, SSA and Asymmetry factor	Sunphotometer
Surface albedo	Sunphotometer
W	Sunphotometer
O ₃	OMI/AURA Satellite
CBH	Ceilometer
r _e and LWC	Literature (Kampe, 1950; Hess et al., 1998; Nimnuan et al., 2017)
Solar spectral irradiance	Spectroradiometer

3.1.2 Methodology

To determine the optical thickness of the cloud (COT), we used the method of Serrano et al. (2015) and all data in Nakhon Pathom. First of all, the required data from the aforementioned instruments in 2019–2020 were collected. After that, the radiative transfer model called "LibRadtran" (Library for Radiative transfer) (Mayer et al., 2012) was used to determine the COT. Figure 14 shows a chart for the determination of the optical thickness of clouds.

For the method to determine COT, we used solar irradiance from spectroradiometer in 19 wavelengths covering ultraviolet wavelengths (310, 340, 380 and 400 nm), visible wavelengths (440, 500, 550 and 700 nm) and near-infrared wavelengths (800, 850, 900, 1050, 1100, 1200, 1300, 1500, 1550, 1600 and 1700 nm). From the sky camera, we selected data only when the sky is under overcast condition which was completely covered by a single layer cloud and there was no rain. Subsequently, the values of various variables of the atmosphere, such as the O₃,

W, AOD, SSA, asymmetry factors, surface albedo, θ_z and cloud properties were inputted into the radiative transfer model. The COT value used in the model is set from a default value of 1.0. Then, the model calculates the spectral solar irradiance ($I_{\lambda, \text{model}}$). The $I_{\lambda, \text{model}}$ from the model was compared with spectral solar irradiance measured by the spectroradiometer ($I_{\lambda, \text{meas}}$). If the differences of both spectral solar irradiance were greater than 2.0 percent, the model will adjust the COT values with the increments of 0.2 (δCOT) and recalculate the spectral solar irradiance until $I_{\lambda, \text{meas}}$ obtained from the model are equal to $I_{\lambda, \text{meas}}$ obtained from the spectroradiometer or the difference is less than 2.0 percent. The desired COT is considered at this condition (Figure 14).

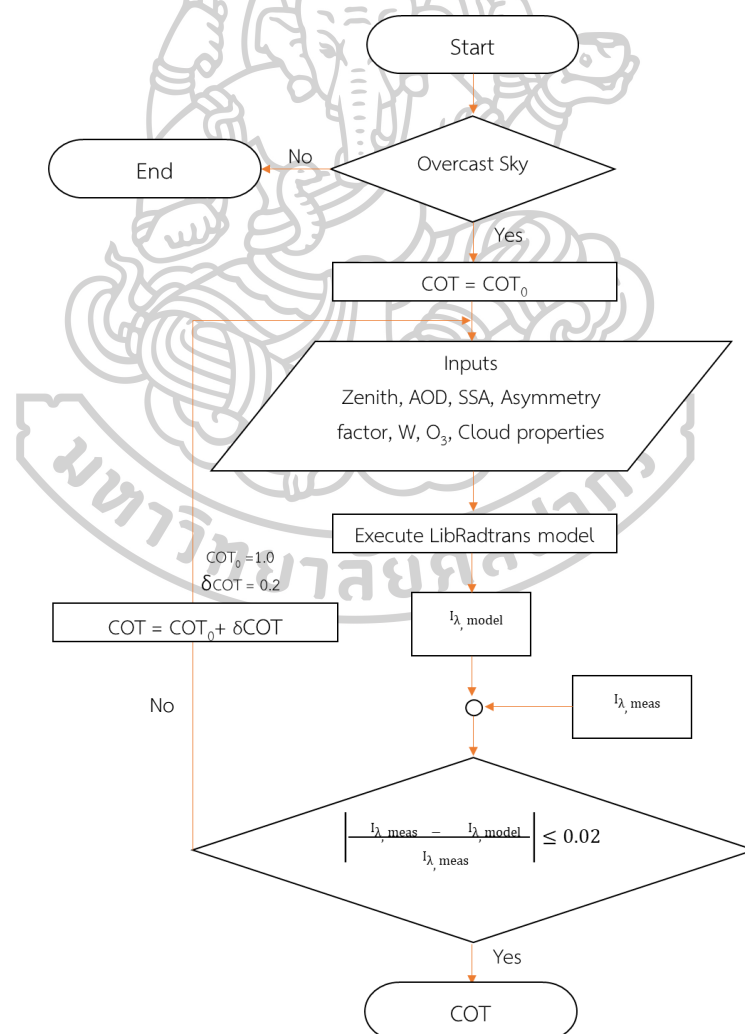


Figure 14 Cloud optical thickness determination process

3.1.3 Results

Examples of spectral solar irradiance collected by the spectroradiometer at 10.30 a.m. local time for two days in September 2019 were presented in Figure 15. The spectral solar irradiance is less than $1 \text{ W/m}^2/\text{nm}$ on overcast sky. From Figure 15, the spectral solar irradiance on these days were different due to the cloud's layer and path length of the sun. On 2 September, 2019, the skies were covered by a single layer cloud, whereas on 19 September, 2019, the multi-layer cloud, which attenuated more solar radiation than single layer clouds, were observed.

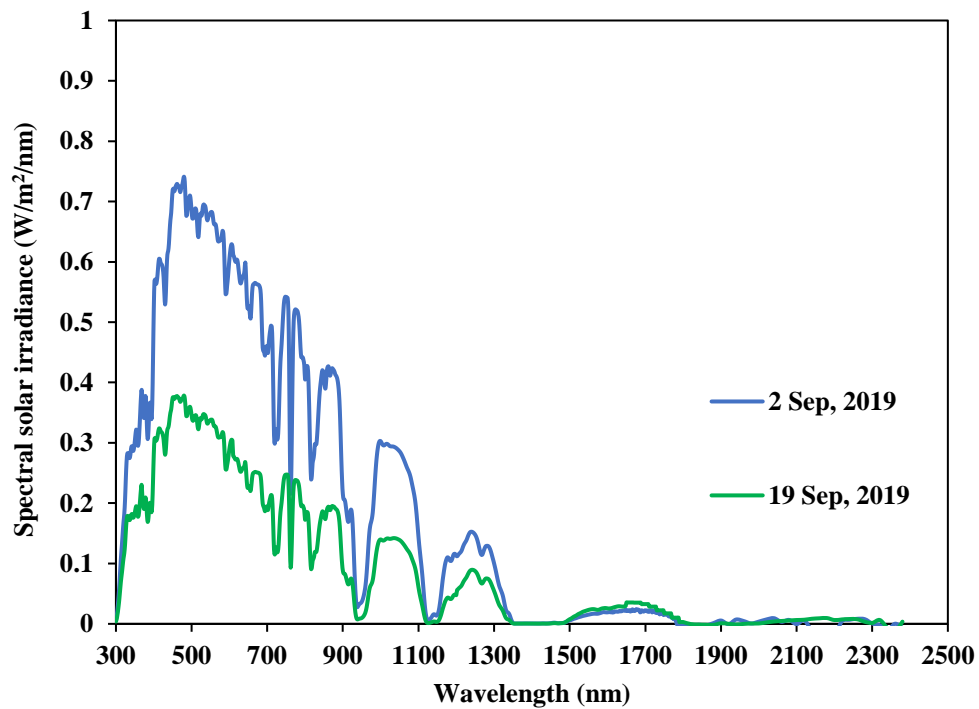


Figure 15 Examples of spectral solar irradiance under overcast sky from the spectroradiometer at 10.30 a.m. local time of different days in September 2019

Examples of the results of COT in low-level cloud show in Figure 16. In these cases, it was seen that the optical thickness of the clouds slightly changed over the wavelengths. However, from the statistical analysis, it shows that COT is independent of wavelength throughout the ultraviolet and visible wavelengths and COT increases

in the NIR wavelength. It was found that the COT in UV and visible wavelengths is similar and COT in NIR is increasing. This finding corresponds to the theory (Serrano et al., 2015).

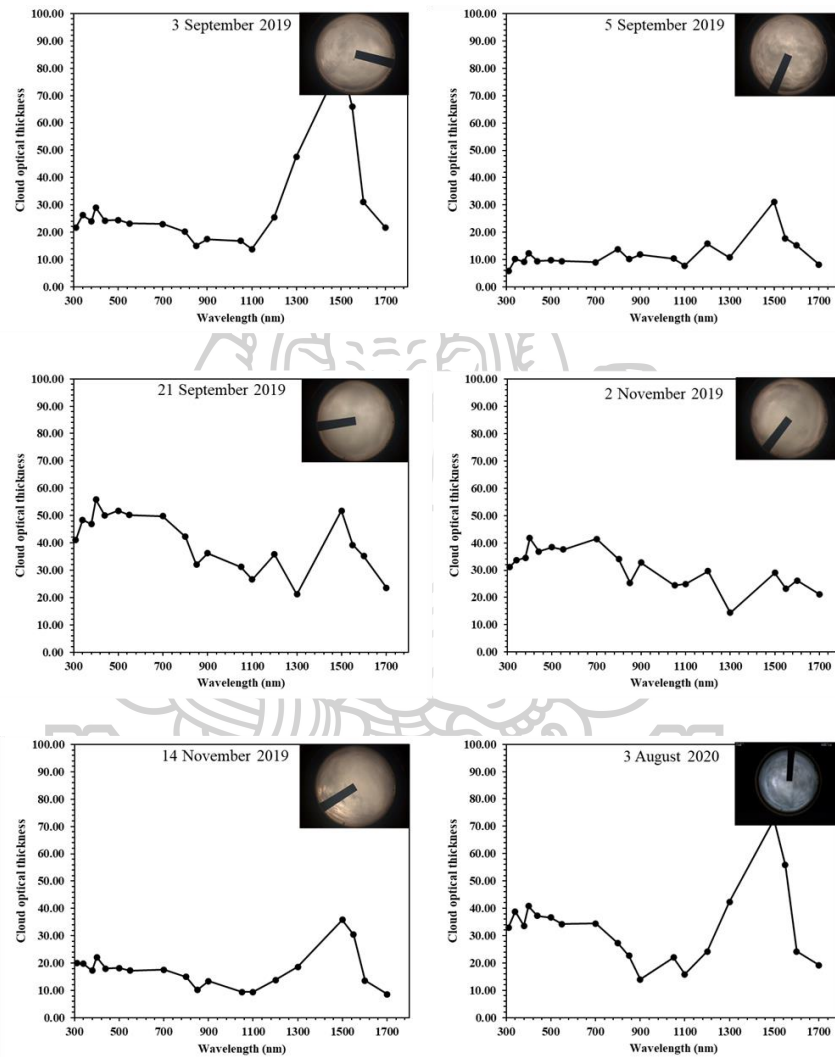


Figure 16 COT in low-level cloud

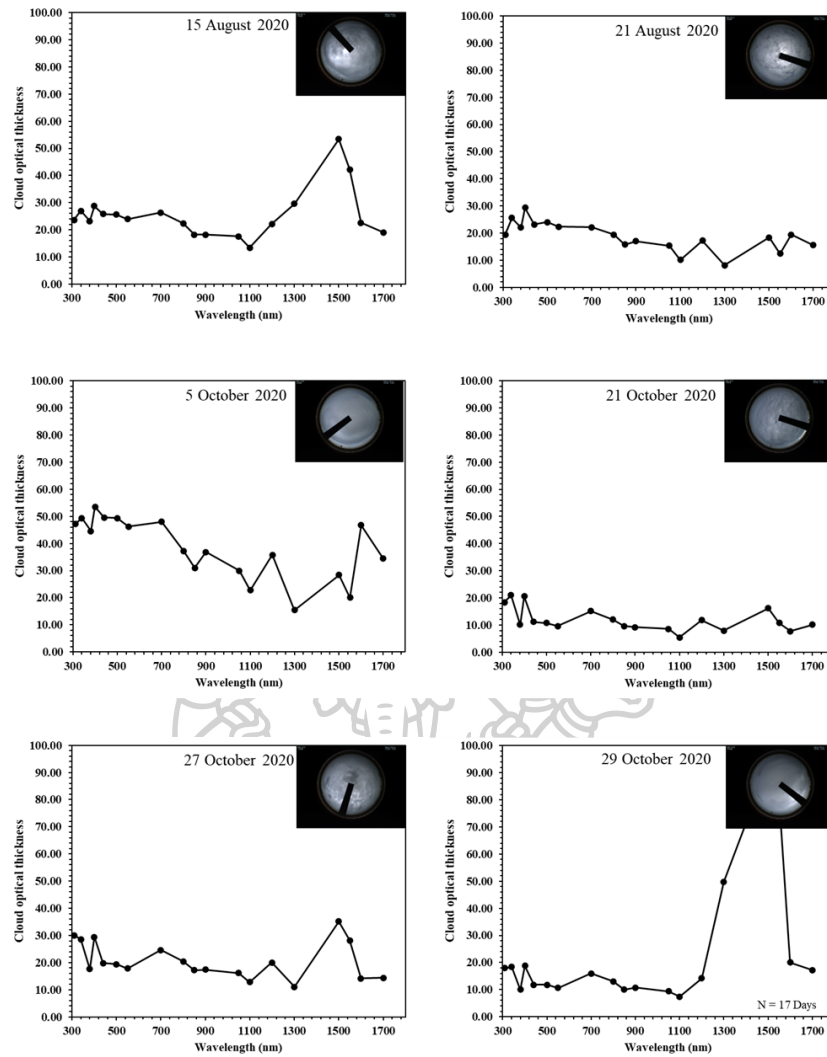


Figure 16 (continue) COT in low-level cloud

3.1.4 Conclusion

Cloud optical thickness (COT) at Nakhon Pathom station (13.82°N, 100.04°E) has been determined using ground-based data and a radiative transfer model. It was found that COT in UV and visible wavelengths are almost the same and COT in NIR wavelengths is increasing compared to COT in UV and visible wavelengths.

3.2 COT and r_e mapping over Thailand by using satellite data

This research will study the cloud optical thickness and cloud effective radius by using satellite data, which are important parameters for determining the attenuation of the solar radiation reaching the Earth's surface and are indicators of the cloud's nature to produce rain. The method used in this work is adapted from Nakajima et al. (1995). In principle, we can find COT and r_e from measurements by aircrafts or ground-based instruments, but such measurements are so expensive and do not cover all areas. Therefore, a method for determining COT and r_e from satellite data is used in this work. The details of the work are as follows.

3.2.1 Satellite data

To determine COT and r_e , the data from Himawari-8 satellites was used. Table 4 shows the details of data of the Advanced Himawari Imager (AHI). The data used in this work are in band 2 ($0.51 \mu\text{m}$), band 7 ($3.9 \mu\text{m}$) and band 13 ($10.4 \mu\text{m}$). The time interval of the satellite image data was used from January 2016 to December 2020. Figure 17 shows an example of satellite data from band number 2, 7 and 13 covering Thailand.

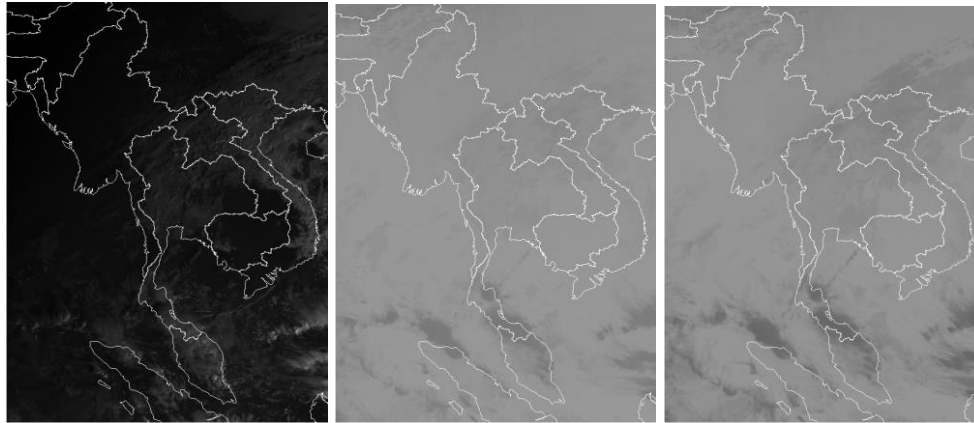


Table 4 AHI observation bands

Wavelengths (μm)	Himawari-8		
	Band number	Spatial resolution at SSP** (km)	Central wavelength (μm)
0.47	1	1	0.47063
0.51*	2	1	0.51000
0.64	3	0.5	0.63914
0.86	4	1	0.85670
1.6	5	2	1.6101
2.3	6	2	2.2568
3.9*	7	2	3.8853
6.2	8	2	6.2429
6.9	9	2	6.9410
7.3	10	2	7.3467
8.6	11	2	8.5926
9.6	12	2	9.6372
10.4*	13	2	10.4073
11.2	14	2	11.2395
12.4	15	2	12.3806
13.3	16	2	13.2807

*bold character indicates the bands used

**SSP is Sub Satellite point



(a)

(b)

(c)

Figure 17 Satellite data from (a) band number 2, (b) band number 7 and (c) band number 13

The value from the satellite in band 2 is the reflectivity. We have to convert this value to radiance (unit: $W/m^2/sr/\mu m$). For band 7 and 13, it is the brightness temperature value or TB (unit: K) and this value will be also converted into radiance. The conversions are based on the calibration tables from the Japan Meteorological Center of JMA. The calibration graphs of the three bands show in Figure 18-20.

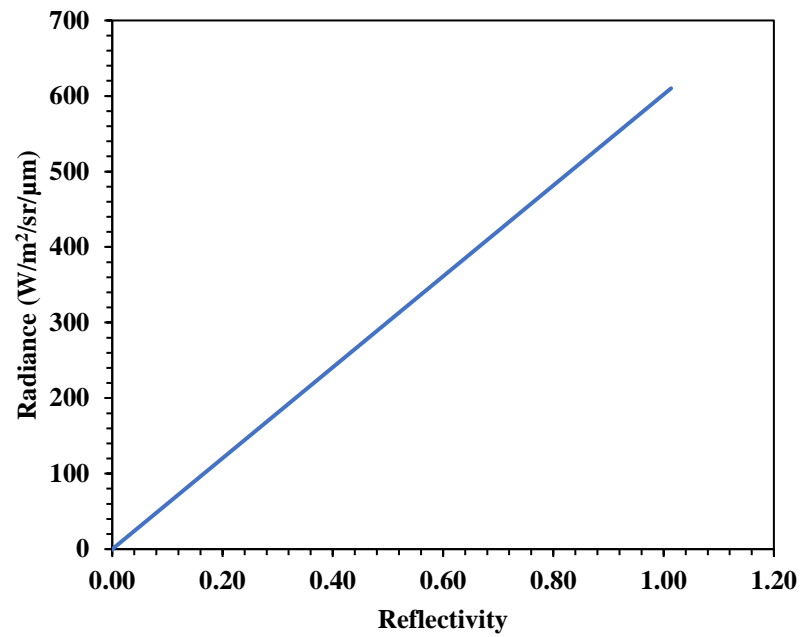


Figure 18 Correlation between reflectivity and radiance from band 2

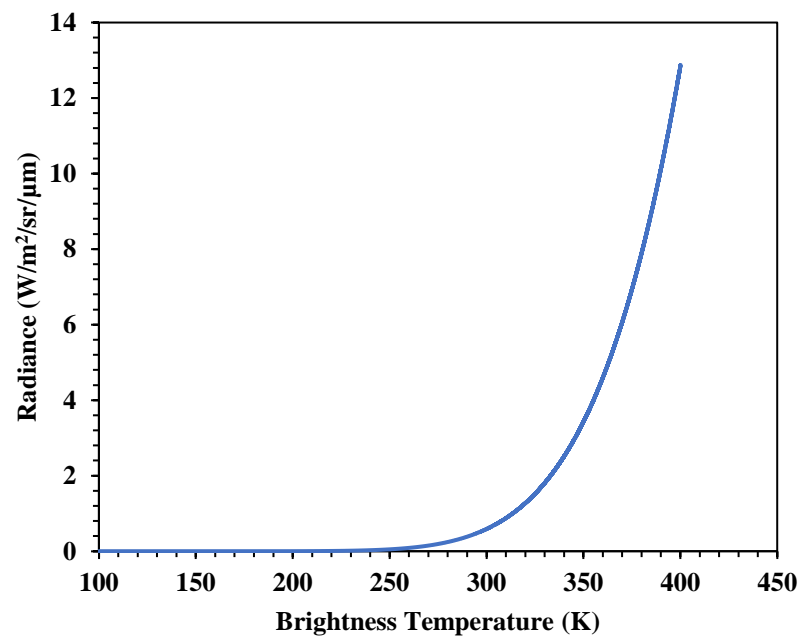


Figure 19 Correlation between brightness temperature and radiance from band 7

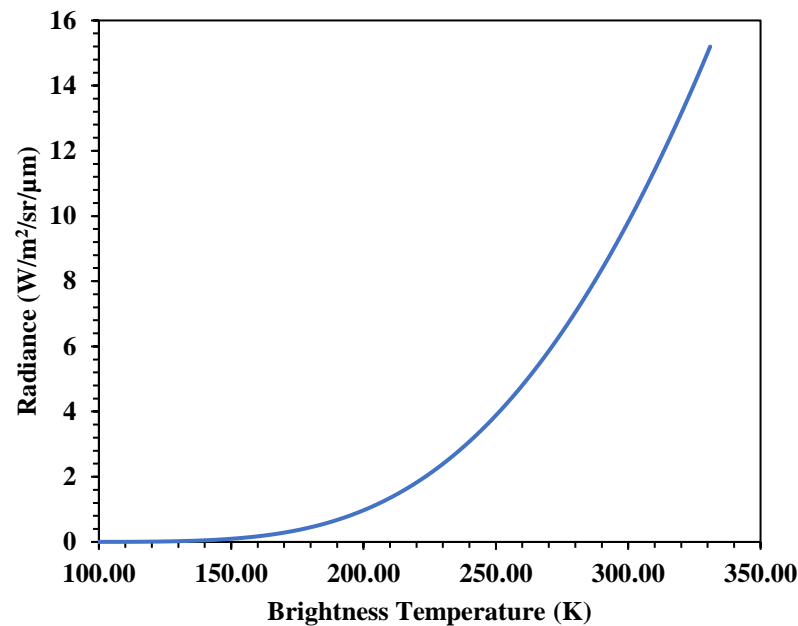


Figure 20 Correlation between brightness temperature and radiance from band 13

3.2.2 The determination for COT and r_e from satellite data

In the first step for the determination of the COT and r_e , we created three Look Up Tables (LUTs); LUT-A, LUT-B and LUT-C, by using the SBDART (Santa Barbara DISORT Atmospheric Radiative Transfer) radiative transfer model. We use the SBDART model because it is a FORTRAN computer code designed for the analysis of a wide variety of plane-parallel radiative transfer problems encountered in satellite remote sensing and atmospheric energy budget studies (Ricchiuzzi et al., 2000). From the model, it can determine cloud top height (Z), cloud geometrical thickness (D), cloud effective radius (r_e), cloud optical thickness (COT), azimuth angle of satellite (ϕ), zenith angle of satellites (θ) and the zenith angle of the sun (θ_z).

In this work, the SBDART model was used to determine the cloud reflectance ($L_{m,0.51 \mu m}$) at a wavelength of $0.51 \mu m$ and $L_{m,3.9 \mu m}$ at a wavelength of $3.9 \mu m$ for LUT-A and LUT-B, respectively. The parameters required for the model are shown in Table 5. Zenith angle and azimuth angles of the satellite can be calculated from the satellite's position and the height of the satellite above the earth. LUT-C is a table showing the relationship between the ratio of cloud base radiation (L_{cloud}) to

terrestrial radiation (L_{surf}) or t_c at a wavelength of $10.4 \mu\text{m}$ at different cloud base height (H).

Table 5 Values of parameters in LUT-A and LUT-B

Parameters	Values
COT	0,1,2,3,...,99,150
r_e	2,3,...,99,100
D	0.1,0.2,0.5,1.0,2.0
Z	1.0,1.5,2.0,...,12.0
θ_z	0,5,10,20,30,35,40,45,50,55,60,65,70
θ	48.33°
ϕ	290.78°

Figure 21 shows the method to determine COT and r_e where Z is the cloud top height, t_c is the ratio of cloud base radiation to the terrestrial radiation, T_c is the cloud top temperature, T_s is the surface temperature, D is the cloud geometrical thickness, COT is the optical depth of the cloud, r_e is the cloud effective radius, θ is the zenith angle of the satellite, θ_z is the zenith angle of the sun and ϕ is the azimuth angle of the satellite, $L_{m,0.51 \mu\text{m}}$ is the cloud reflectance at $0.51 \mu\text{m}$ wavelength obtained from LUT-A, $L_{m,3.9 \mu\text{m}}$ is the cloud reflectance of the $3.9 \mu\text{m}$ wavelength obtained from LUT-B, $L_{obs,0.51 \mu\text{m}}$ is the cloud reflected value obtained from satellite data in band number 2, $L_{obs,3.9 \mu\text{m}}$ is the cloud reflectance value obtained from satellite data in band number 7, and $L_{obs,10.4 \mu\text{m}}$ is the earth reflectance value obtained from satellite data in band number 13.

Initially, COT, r_e and Z are set to 35, $10 \mu\text{m}$ and 2 km, respectively. Cloud geometrical thickness (D) is calculated from the equation.

$$D = \frac{LWP}{LWC} \tag{4}$$

where D is the cloud thickness
 LWC is liquid water content
 LWP is liquid water path.

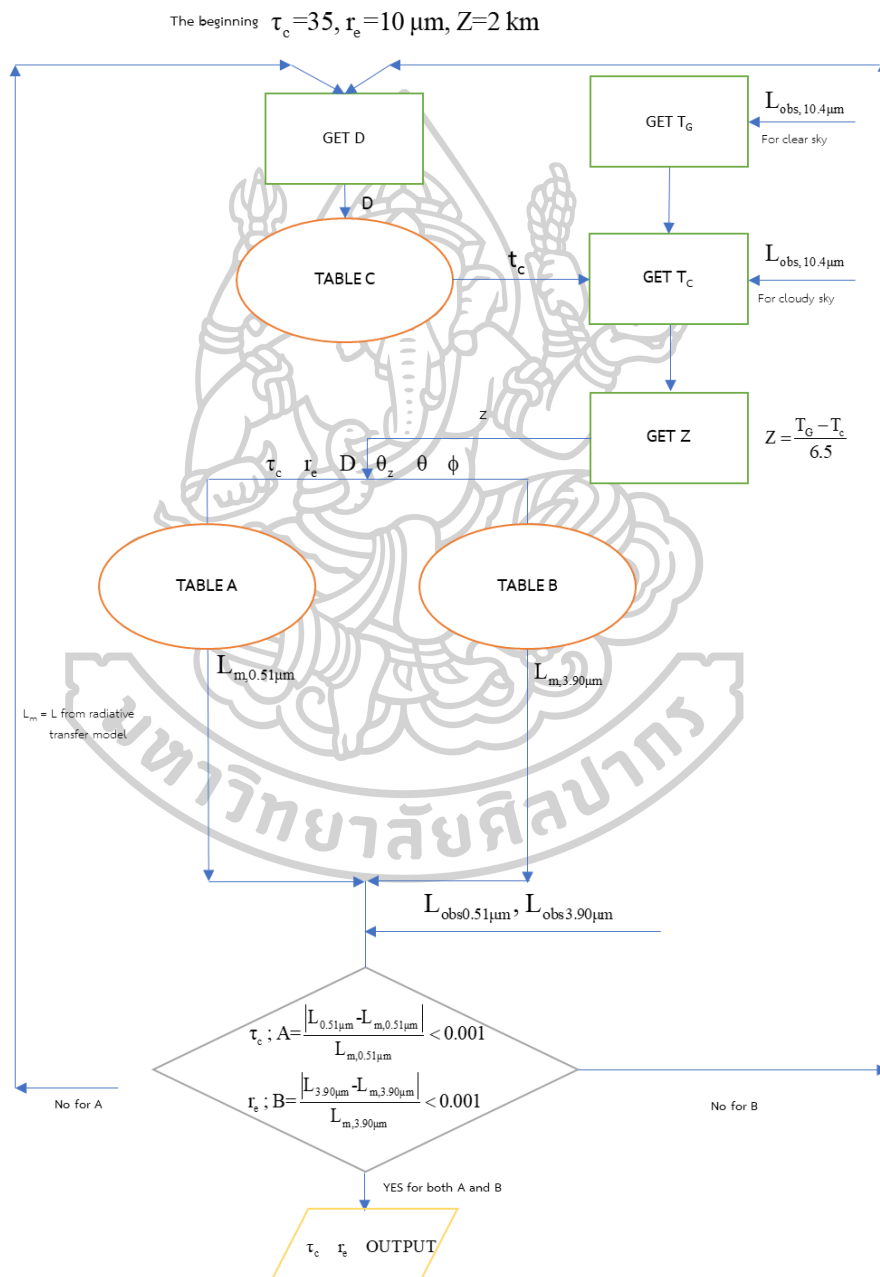


Figure 21 Diagram showing the algorithm to determine COT and r_e adapted from Nakajima et al. (1995)

The value D can get from Equation (4) and the value of cloud base height is calculated as $H=Z-D$. Thus, t_c was obtained from LUT-C, and then the t_c value was used to determine cloud top temperature (T_c)

$$T_c = \frac{c_2 \nu}{\ln\left(\frac{c_1 \nu^3}{BT_c} + 1\right)} \quad (5)$$

where c_1 is $2h/c^2$ ($h = 6.62620 \times 10^{-34}$ J.s)

c_2 is h/kT_G ($k = 1.38062 \times 10^{-23}$ J.K⁻¹)

ν is frequency (cm⁻¹)

BT_c is cloud top radiation (mW.m⁻².sr⁻¹.cm⁻¹)

c is speed of light (3×10^8 m.s⁻¹).

Then the T_c values were used to calculate the true value of Z . This is because the height of the cloud tops was initially set as the default only. To find the cloud top height, we used the equation

$$Z = \frac{T_G - T_c}{6.5} \quad (6)$$

where Z is cloud top height (km)

T_G is surface temperature on clear sky day (K)

T_c is cloud top temperature (K).

We can use LUT-A to determine cloud reflectance at a wavelength of 0.51 μm ($L_{m,0.51 \mu\text{m}}$) and LUT-B to obtain cloud reflectance at a wavelength of 3.9 μm ($L_{m,3.9 \mu\text{m}}$). These values were compared with the reflected cloud values obtained from the satellite data in the band number 2 ($L_{\text{obs},0.51 \mu\text{m}}$) which is in the visible band, and band number 7 ($L_{\text{obs},3.9 \mu\text{m}}$) which is in the near-infrared band according to the equation:

$$\mathbf{A} = \left| \frac{L_{\text{obs},0.51 \mu\text{m}} - L_{m,0.51 \mu\text{m}}}{L_{m,0.51 \mu\text{m}}} \right| \quad (7)$$

$$\mathbf{B} = \left| \frac{L_{\text{obs},3.9 \mu\text{m}} - L_{m,3.9 \mu\text{m}}}{L_{m,3.9 \mu\text{m}}} \right|$$

It is determined that A and B should be not more than 0.02. If A exceeds 0.02, we will adjust the COT and then calculate again. Similarly, if B exceeds 0.02, r_e is adjusted. The loop calculations were performed over and over until A and B values do not exceed 0.02. The COT and r_e values that make both A and B less than 0.02 are true COT and r_e values.

This algorithm was used to obtain the COT and r_e of each satellite pixel covering the region of Thailand. The example results of January 1, 2017, at 8:30 a.m. are presented as maps (Figure 22).

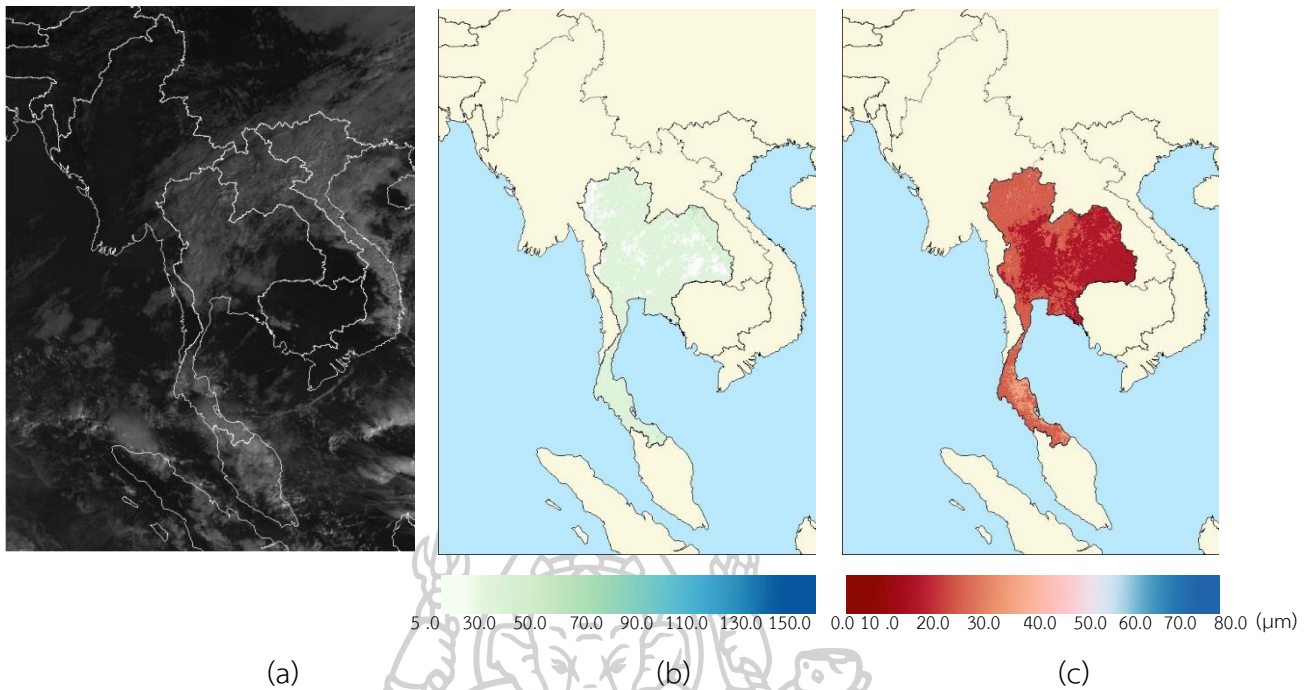


Figure 22 Mapping of COT and r_e values obtained from satellite data on 1 January 2017 at 8.30 a.m. (a) satellite imagery in band number 2 (Visible wavelength), (b) COT mapping and (c) r_e mapping.

Figure 22(a) is the satellite imager in the visible band. The corresponding COT and r_e are shown in Figure 22(b) and (c), it can be seen from the maps that the COT values are in the range of 5-50 and r_e are between 10-40 μm .

3.2.3 Statistical analysis of COT and r_e

We studied the statistical characteristics of the monthly average of COT and r_e during 2017 (Figure 23 and 24).

Figure 23 shows the monthly average of the COT values for 2017. The maps show the variations of COT from month to month of the year. From January to March, in the Northern, Central and Northeast regions, the lowest values for cloud optical depth are in the range of 0-20 and the lowest values are shown during February. For the months of April to September, the COT is approximately 15-60 and found that the optical depth of clouds is around 25-50 in most of the whole Thailand in September. From October to December, the COT decreases again. In the Southern region, the COT is around 15-60 throughout the year.

Figure 24 shows the monthly average of the r_e values for 2017. The maps also show the change of r_e during the year. During the months of January to April, r_e is small in most region except in Southern region. This small r_e is in the range of 0-20 μm and it shows the lowest value during February. From May to September, the r_e is about 20-30 μm and the values increase to about 30-40 μm in most regions of Thailand in July. During October to December, r_e decreases for all regions except in the Southern region where the r_e is still in the range of 20-40 μm .

From the results of COT and r_e in the year 2017, the values of COT and r_e were comparable with those received from MODIS satellite in the same year.

3.2.4 Conclusion

Cloud optical thickness (COT) and effective radius (r_e) over Thailand have been mapped using Himawari-8 satellite data during 2016-2020. It was found that COT is lowest from January to March and increases from April to October in the Northern, Central and Northeast of Thailand. After that, in November and December the COT and r_e decrease. For Southern of Thailand, the COT and r_e are high for all seasons.

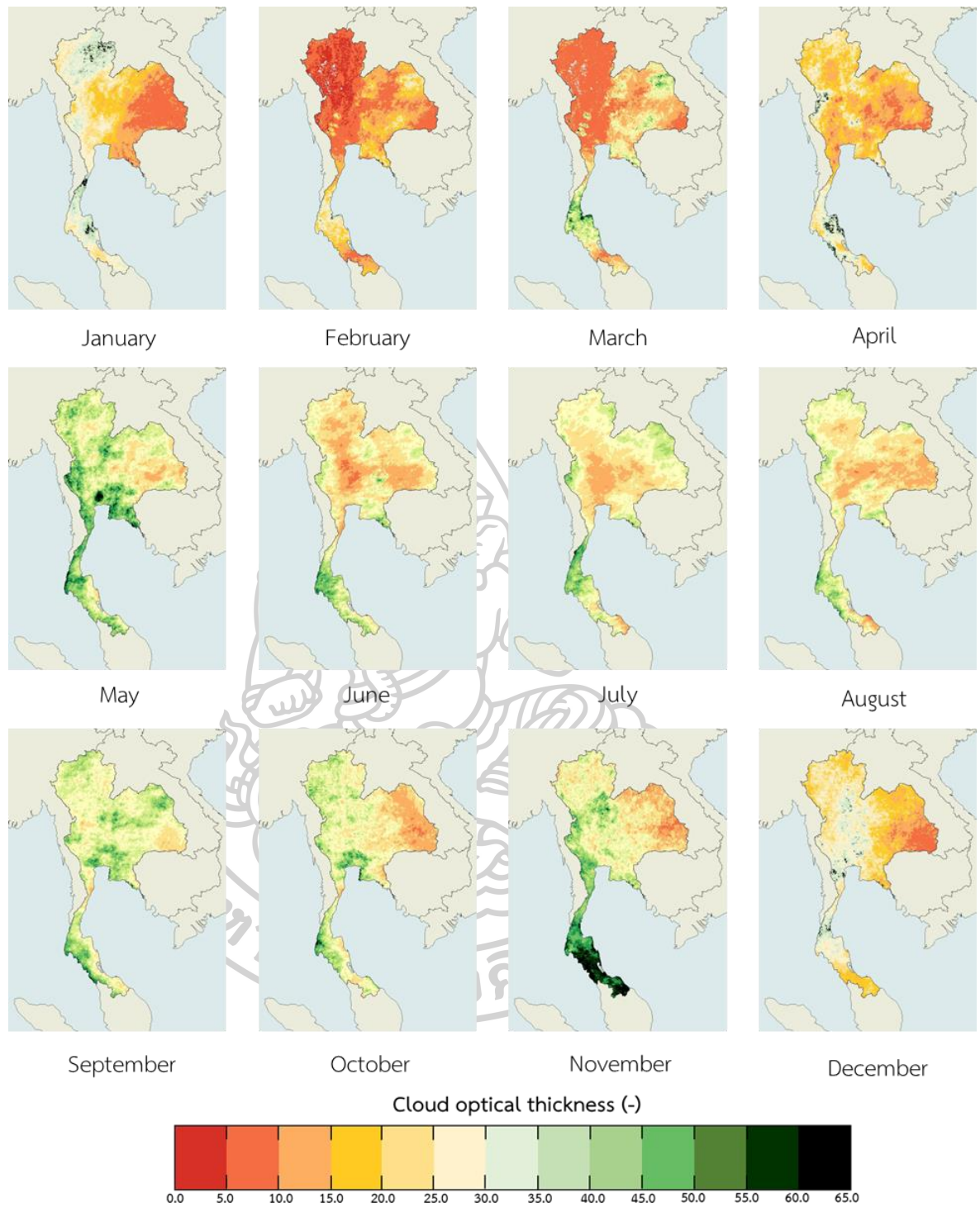


Figure 23 Monthly average cloud optical thickness over Thailand

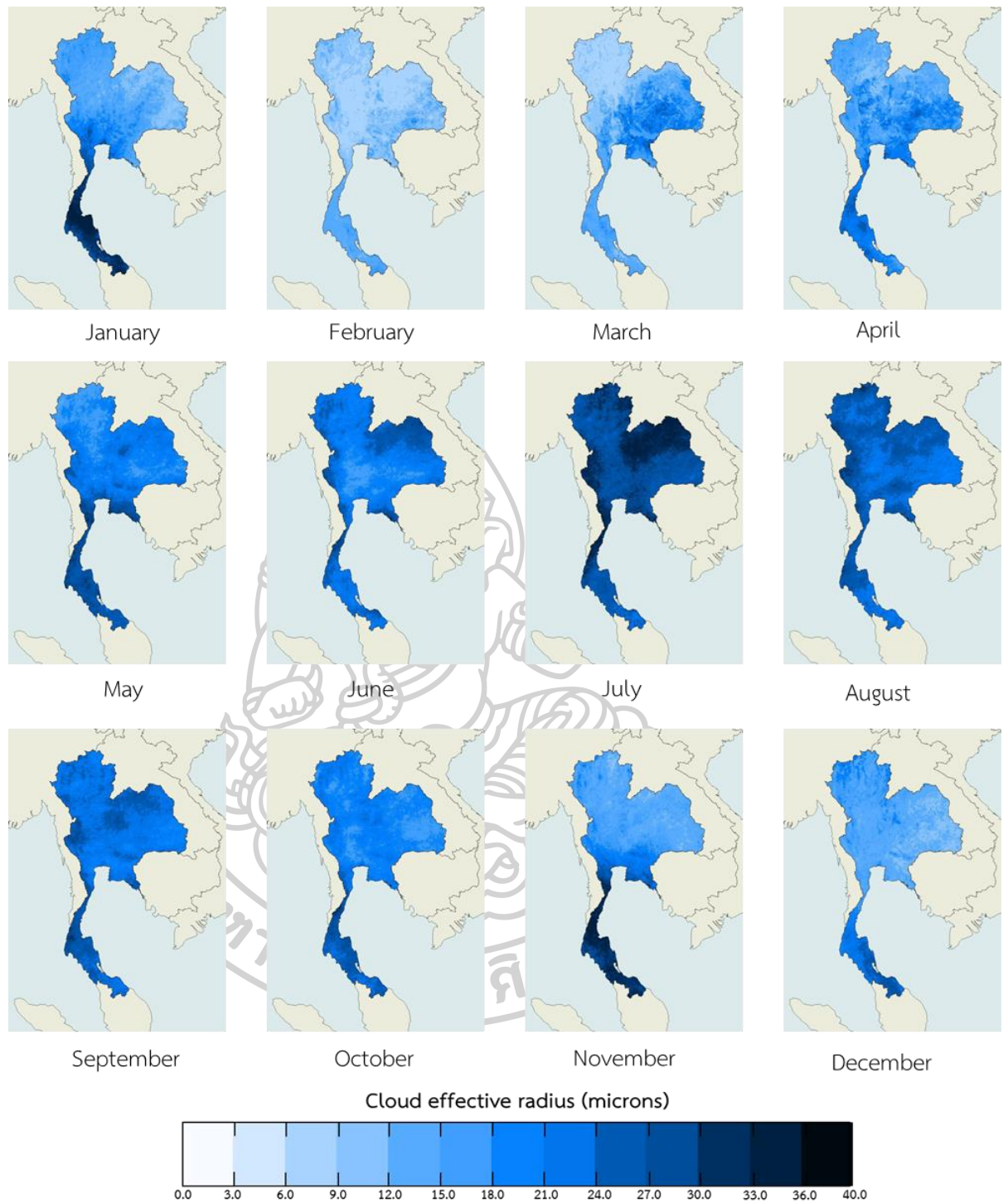


Figure 24 Monthly average cloud effective radius over Thailand

3.3 Cloud cover from satellite data over Thailand¹

In this study, an empirical model for estimating cloud cover from satellite data was developed. The skyview instruments were installed at four stations located in Chiang Mai (18.78°N, 98.98°E), Ubon Ratchathani (15.25°N, 104.87°E), Nakhon Pathom (13.82°N, 100.04°E) and Songkhla (7.20°N, 100.60°E) in order to record the images of the sky. A five – year period (2009 – 2013) of the cloud cover derived from the sky images and cloud index derived from MTSAT–1R satellite data were acquired. Based on these data, a model relating the cloud cover to the cloud index was formulated. To validate its performance, the model was used to calculate cloud cover at the four stations during a two-year period (2014 – 2015).

3.3.1 Methodology

The mapping process of cloud cover consists of five main steps, namely derivation of cloud cover from sky images, processing of satellite data, model validation and mapping. The details of each step are described as follows.

3.3.1.1 Derivation of cloud cover from sky images

Determining cloud cover from sky images was achieved from ground-based measurements using skyviews which have been installed at four meteorological stations in Chiang Mai (18.78°N, 98.98°E), Ubon Ratchathani (15.25°N, 104.87°E), Nakhon Pathom (13.82°N, 100.04°E) and Songkhla (7.20°N, 100.60°E), for those representing North, Northeastern, Central and Southern regions of Thailand, respectively (Figure 25). Each skyview was set to capture sky images every five minute and the images were recorded into a PC. The resolution of each image is 640 × 480 pixels.

¹ This topic has been published in the Journal Science, Engineering and Health Studies (2018) 69-76.



Figure 25 A map of Thailand showing the locations of the study sites and the pictorial view of the skyviews used in this work. A, B, C and D indicate the Northern, Northeastern, Central and the Southern regions, respectively.

The sky images from the four stations during 9:00–15:00 of a five-year period (2009 – 2015) were collected. These data were undergone an algorithm that counts the ratio of number of pixels dominated by cloud to number of total sky pixels (Ghonima et al., 2012). The cloud cover data were then processed to monthly average cloud cover. To verify the performance of the algorithm, the monthly average cloud cover from the algorithm were compared with those obtained from visual observation at Chiang Mai and Songkhla stations during 2011-2013. The differences between these datasets can be presented by the percentage of root mean square difference relative to mean observed values (RMSD) and the percentage of mean bias difference relative to mean observed values (MBD). RMSD and MBD are defined as follows.

$$\text{RMSD} = \frac{\sqrt{\frac{\sum_{i=1}^N (C_{y,i} - C_{x,i})^2}{N}}}{\frac{\sum_{i=1}^N C_{x,i}}{N}} \times 100 \quad (8)$$

$$\text{MBD} = \frac{\frac{\sum_{i=1}^N (C_{y,i} - C_{x,i})}{N}}{\frac{\sum_{i=1}^N C_{x,i}}{N}} \times 100 \quad (9)$$

where $C_{y,i}$ is cloud cover derived from the skyview, $C_{x,i}$ is cloud cover from the observation, i is the order of the data ($i = 1, 2, \dots, N$) and N is total number of the data.

The comparison results in Figure 26 show a reasonable agreement, with root mean square difference (RMSD) and mean bias difference (MBD) of 10.1% and -2.7%, respectively.

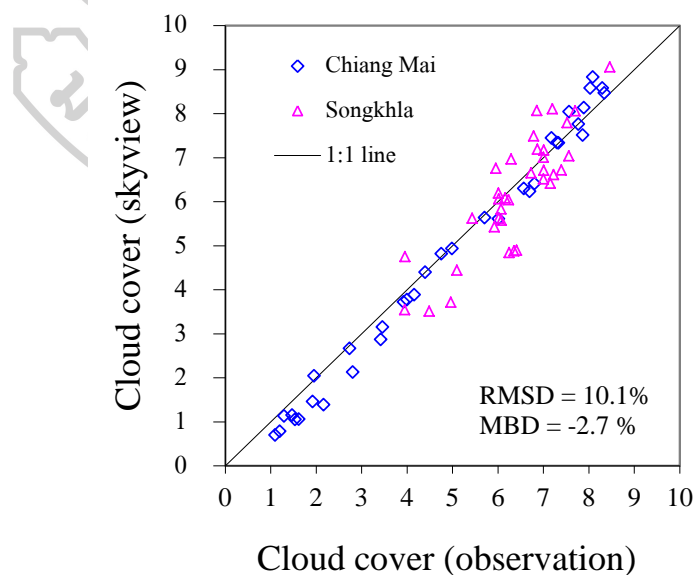


Figure 26 The comparison between monthly average cloud cover from the skyviews algorithm and visual observation

3.3.1.2 Satellite data processing

As satellite images can depict the amount of cloud, in this study, the digital data from a visible channel (0.55 - 0.90 μm) of the MTSAT – 1R satellite during a 10-year period (2006 – 2015) were used. These data covered the entire area of Thailand with a spatial resolution of $3 \times 3 \text{ km}^2$. These images were transformed to the cylindrical map projection and navigated using coastlines as references. Each navigated image consists of 550×850 pixels (Figure 27), each of which has a gray level value from 0 to 255. Then the gray levels of forty-nine pixels (7×7 pixels) centered at the stations were transformed into the pseudo-reflectivity (ρ_{SAT}) by the conversion table provided by the satellite agency (JMA, 2009). In the final step, the pseudo-reflectivity was divided by the cosine of the local solar zenith angle at each pixel in order to obtain earth-atmospheric reflectivity (ρ_{EA}). This earth-atmospheric reflectivity was averaged for the forty-nine pixels centered of each station. These values will be used to estimate cloud index (n), which signify the cloud cover, following the method of Cano et al. (1986) as:

$$n = \frac{\rho_{\text{EA}} - \rho_{\text{G}}}{\rho_{\text{C}} - \rho_{\text{G}}} \quad (10)$$

where ρ_{EA} , ρ_{G} and ρ_{C} are earth – atmospheric reflectivity, ground reflectivity and maximum cloud reflectivity, respectively. The ground reflectivity (ρ_{G}) was estimated by using the satellite images. Monthly composite images were generated to eliminate cloud contamination. Then, these cloud – free images were converted into ground reflectivity (Janjai et al., 2006). In contrast, the maximum cloud reflectivity was estimated from the maximum value of the gray level for each pixel of satellite images all year round. Then, the satellite images with maximum value of the gray level were used to represent the maximum cloud reflectivity for each year.

From Equation (10), when the pixel is cloud-free or $\rho_{\text{EA}} = \rho_{\text{C}}$, $n = 0$ and for the case of overcast condition $\rho_{\text{EA}} = \rho_{\text{G}}$, $n = 1$. Additionally, for the case of party

cloudy condition, $0 < n < 1$. This implies that n indicates indirectly the amount of cloud.

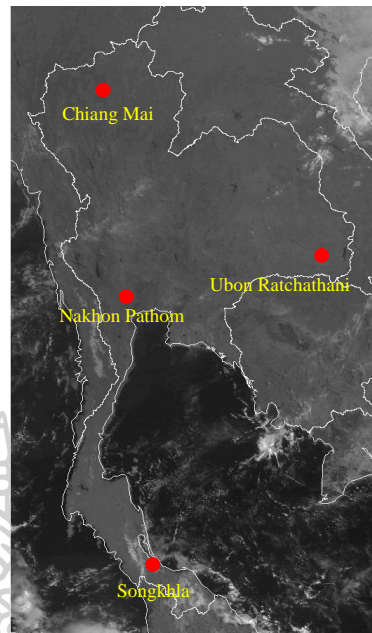


Figure 27 An example of a navigated image and the locations of the ground-based stations

3.3.1.3 Modelling

As cloud index indicates the amount of cloud, the statistical relation between cloud index and cloud cover is expected. To obtain this relation, monthly average cloud cover from the sky images were plotted against monthly average cloud index estimated from the satellite data. These data cover the period of 2009 - 2013 and the results are shown in Figure 28.

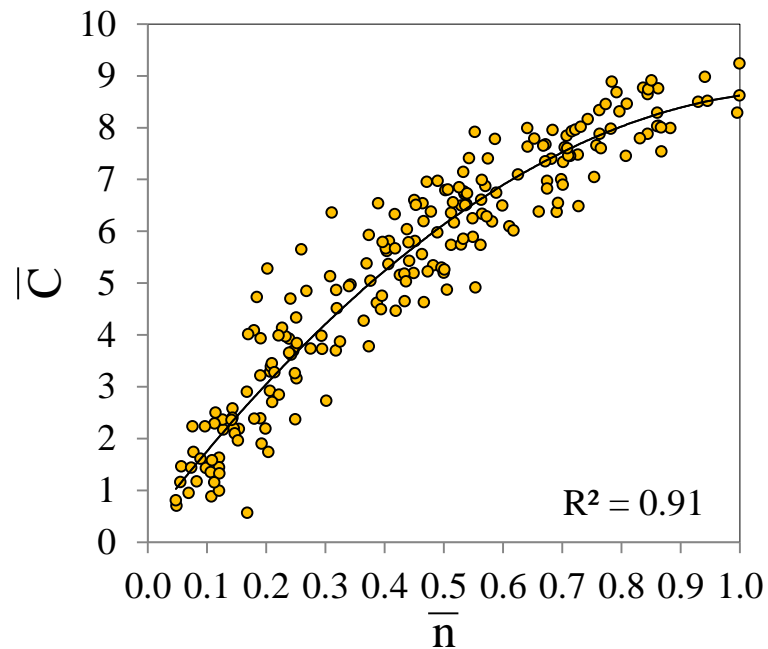


Figure 28 The relation between monthly average cloud cover from the sky images (\bar{C}) and monthly average cloud index (\bar{n}) from the satellite data

The relation in Figure 28 was fitted by the least square technique (Wolberg, 2006) which can be expressed as a quadratic equation:

$$\bar{C} = a_1 + a_2 \bar{n} + a_3 \bar{n}^2 \quad (11)$$

where \bar{C} is monthly average cloud cover, \bar{n} is monthly average cloud index, and a_1 , a_2 and a_3 are empirical constants. The values of these constants and their associated t-statistic are shown in Table 6.

Table 6 The empirical constants and t-statistic

Empirical constant	Value	t-statistic
a_1	0.3368	2.09913
a_2	14.896	19.74949
a_3	-6.611	-8.64677

Table 6 shows that the values of t-statistic are greater than 2, meaning that the predictability of the parameters in Equation (11) are significant at 5% significance level.

3.3.1.4 Model validation

To investigate the model's performance, Equation (11) was used to calculate cloud cover using the satellite data during 2014-2015 at the four ground-based stations in Chiang Mai, Ubon Ratchathani, Nakhon Pathom and Songkhla. The calculated cloud cover values were compared with those measured from the skyviews. The results are depicted in Figure 29 which show the discrepancy in terms of RMSD and MBD of 12.9% and 3.5%, respectively. This result implies that the model performs reasonably well in estimating the cloud cover.

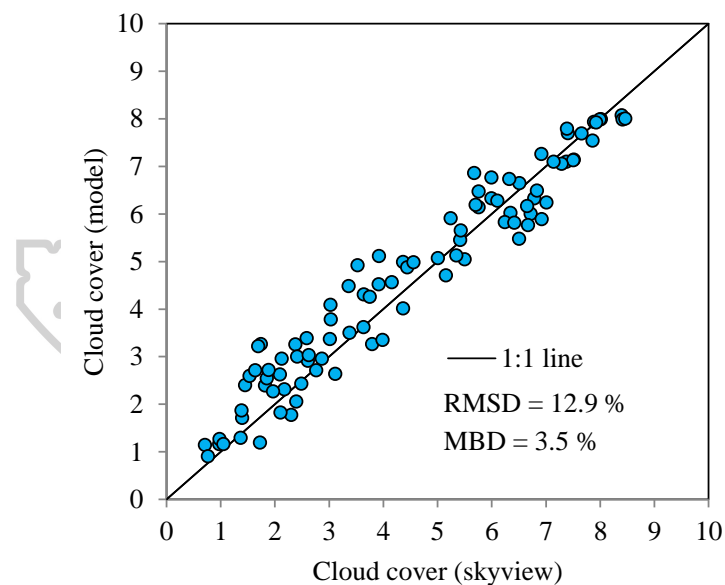


Figure 29 Comparison between cloud cover from the proposed model and that from the sky images at the four stations

3.3.1.5 Mapping of monthly average cloud cover

After the validation, the model was used to estimate cloud cover from the cloud index derived from MTSAT-1R satellite over a period of 10 years (2006 – 2015) and the results are displayed as maps.

3.3.2 Results and discussion

The monthly average and yearly average maps of cloud cover of Thailand are shown in Figure 30 and 31, respectively.

Figure 30 shows monthly average cloud cover over a 10-year period (2006 – 2015). The seasonal variation is explicitly observed, which corresponds to several atmospheric factors, e.g., atmospheric water vapor and aerosols as well as seasonal meteorological conditions. During January to February, the Northern, the Northeastern and Central regions of Thailand have less cloud cover because the East Asian monsoon brings cold and dry air into these areas. Meanwhile the East Asian monsoon blows moist air from the Gulf of Thailand to the Southern region, resulting in more cloud cover in this region.

Even during the calm period between March and April, cloud cover starts to show up in the lower Central Thailand. This would be caused by the trough, which spans over that area. In May, the South Asian monsoon starts to blow across the Indian Ocean and initiates the rainy season, which continue until October. This results in more cloud cover occurring over the country.

During November to December, the cloud cover distribution is quite similar to January-February as they are also under the influence of East Asian monsoon. However, cloud cover over the southern area is much more intensifying due to this monsoon blowing across the Gulf of Thailand.

In Figure 31, the annual average cloud cover over years 2006 – 2015 is presented. Since the southern Thailand is surrounded by the sea and is influenced by both East and South Asian monsoons, the annual average cloud cover in this region is the highest. The higher cloud cover in the western shore of the southern Thailand is likely caused by local topography of this area. This orographic rain

landscape is also found in the Eastern Thailand, which is also under the influence of the South Asian monsoon.

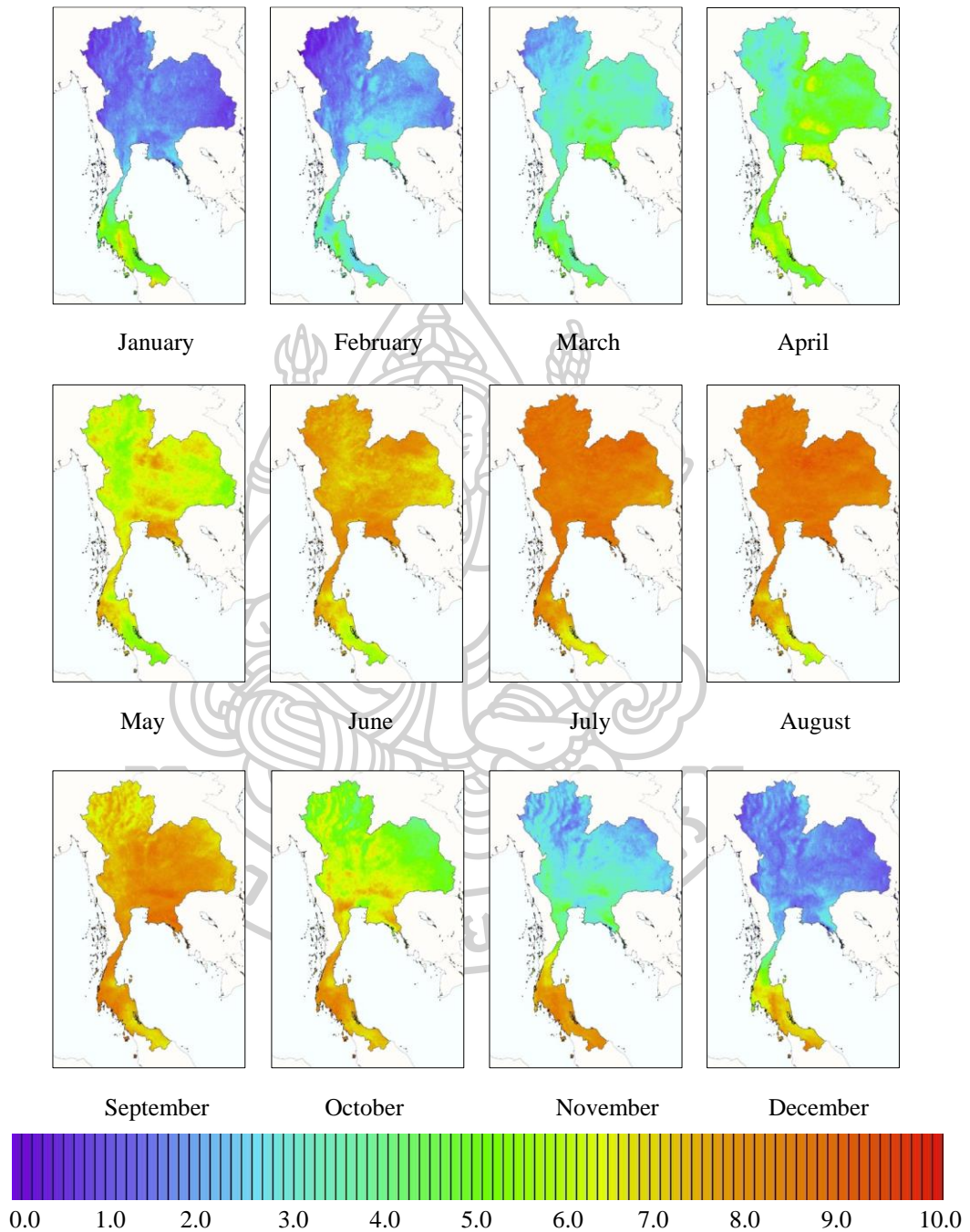


Figure 30 Monthly average cloud cover over Thailand (color code: 0 represents clear sky and 10 is completely overcast)

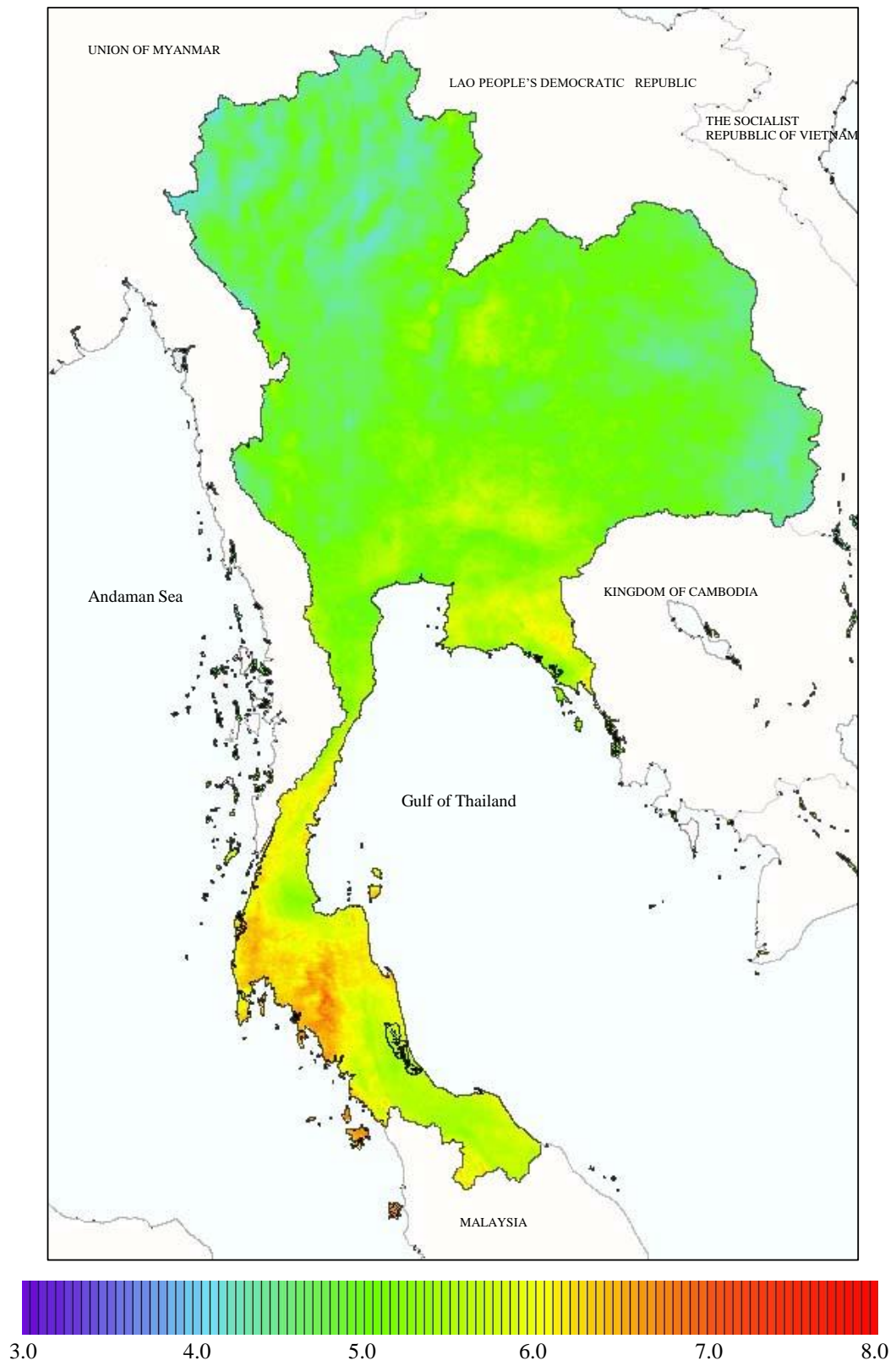
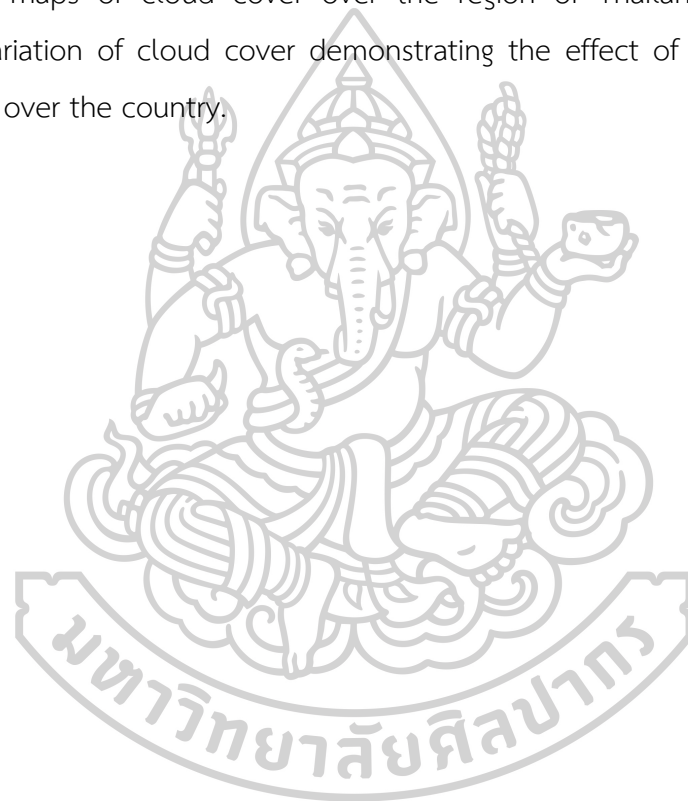


Figure 31 Long-term yearly average cloud cover over Thailand

3.3.3 Conclusion

An empirical model for estimating cloud cover over Thailand from satellite data was developed. The model relates the monthly average cloud cover to the satellite – derived cloud index. This model was validated against the ground-based measurement. The cloud covers from the two datasets were in good agreement with the root mean square difference (RMSD) and the mean bias difference (MBD) of 12.9% and 3.5%, respectively. This model was used to generate long-term monthly and yearly maps of cloud cover over the region of Thailand. The maps show seasonal variation of cloud cover demonstrating the effect of monsoon and local topography over the country.



CHAPTER 4

CONCLUSIONS

In this study, there are three parts. The first part is to estimate the COT and r_e under overcast sky condition in 2019-2020 at Nakhon Pathom site. This work used spectral solar irradiance covering ultraviolet to near-infrared wavelength ranges from a spectroradiometer and several atmospheric parameters such as aerosol optical depth, ozone, water vapor and surface albedo, together with the LibRadtran radiative transfer model to obtain the COT. It was found that the COT in UV and visible wavelengths are similar and COT in the NIR wavelength is increased as compared to UV and visible wavelengths. This finding corresponds to the theory.

The second part of the work is to generate the maps of the properties of clouds that are COT and r_e over Thailand from the satellite data. The Himawari-8 satellite data during 2016-2020 were used in this work. The SBDART radiative transfer model was chosen to determine of COT and r_e . The COT and r_e were obtained and displayed as monthly maps. The maps show the variation of COT and r_e during the year.

Finally, the method for estimating the amount of cloud from satellite (MTSAT-1R) data was developed. The model shows the amount of cloud as a function of satellite cloud index. This work used the cloud amount taken from the ground-based skyviews and the cloud index from the satellite data for the modelling. For the model validation, the cloud amount estimated from the model were compared with that from the measurement. The results of the model validation are in terms of root mean square difference (RMSD) and mean bias difference (MBD). The RMSD and MBD was found to be 12.9% and 3.5%, respectively. After the validation, the model was used to estimate cloud amount over Thailand during the years 2006-2015 and presented as monthly and yearly maps. These maps show the temporal and spatial distributions of cloud amount over Thailand.

Appendix

Comparison of solar spectrum from measurements and that from radiative transfer model under overcast sky condition²

Abstract. The solar spectrum under overcast sky condition is of importance for determining the optical properties of cloud by using a radiative transfer model. In this study, solar spectrum under overcast sky condition was measured by employing a spectroradiometer (Instrument System, model SP-320) at Nakhon Pathom station (13.82 °N, 100.04 °E), Thailand. The wavelength range of the measurements is 220-2400 nm, with the resolution of 1 nm in the wavelength range: 220-1700 nm and the resolution of 20 nm in the wavelength range: 1700-2400 nm. The overcast sky condition is determined by using the images of the sky taken by an automatic sky camera. Fifteen datasets of the solar spectrum were compared with those calculated by a radiative transfer model called “LIBRADTRAN”. The input data of the radiative transfer model were obtained from both measurements and literature. As part of the input data, aerosol optical properties were obtained from an AERONET sunphotometer, total ozone column from OMI/AURA satellite and cloud base height from a ceilometer. It was found that the solar spectrum from the measurements and that from the calculation are in reasonable agreement, with the discrepancy in terms of root mean square error (RMSE) of $0.043 \text{ W}\cdot\text{m}^{-2}\cdot\text{nm}^{-1}$. This comparison indicates that this radiative transfer model is accurate enough for use in determining the optical properties of clouds.

² This chapter has been published in the Journal of Physics: Conference Series (2021) Vol. 1719, No. 1, p. 012032

1. Introduction

The solar radiation incident at the earth's surface is an electromagnetic wave which has a wavelength covering mainly from 300 to 3000 nanometers. It can affect the atmosphere and the global energy balance on the earth's surface. When the solar radiation passes through the earth's atmosphere, it was attenuated by atmospheric constituents such as ozone, water vapor, aerosols, gases and cloud via the absorption and scattering processes. Cloud plays an important role in decreasing of surface solar energy. However, it is very difficult to investigate the properties of cloud because they change all the time. Therefore, there were many researchers who determined properties of cloud and its impacts on solar radiation.

Page [1] found that the solar irradiance under overcast sky was changed, depending on the cloud base height, cloud types, and droplet density of clouds. Kasten and Czeplak [2] studied the types of clouds that affect the global solar radiation at Hamburg, Germany. Their results showed that the solar irradiance under overcast sky was changed, depending on solar zenith angle and types of clouds. Matuszko [3] observed that when the solar radiation reaches the earth's surface, it would not be reduced by the high-level clouds such as cirrostratus. On the other hand, the direct solar radiation was reduced by the low-level clouds and mid-level clouds, namely nimbostratus. Moreover, they were also found that different cloud types could cause the difference in solar irradiance about $700 \text{ W}\cdot\text{m}^{-2}$. In case of spectral solar radiation on cloudy sky, Nann and Riordan [4] investigated a spectral transmission of clouds and proposed the relationships between cloud thickness and its transmittance in the ultraviolet region of the solar spectrum. Then, they were employed for predicting spectral irradiance. Clouds are a crucial factor affecting the variations of spectral solar irradiance and most studies in the past were carried out under atmospheric conditions in middle and high latitudes and the study in the tropics is very limited [6]. Therefore, this study aims to use a radiative transfer model to estimate spectral solar irradiance under overcast sky by using the input data of cloud and other atmospheric properties in the tropics and then compared the results with those obtained from measurements.

2. The instruments and data

Main instruments used in this work were installed at Silpakorn University (13.82° N, 100.04° E), Nakhon Pathom, Thailand (Figure 1) and the data from these instruments encompass a period: August – December 2019. We used the data under overcast sky which was completely covered by a single layer cloud and there was no rain. The sky condition was identified by using sky images taken by a sky camera (PREDE, model: PSV-100). The cloud base height (CBH) was measured by a ceilometer (Campbell Scientific, model: CS135). This ceilometer uses the NIR laser at wavelength of 905 nm which can observe four layers of the cloud base height up to 10 km (Figure 1(b)).

Besides the CBH, other inputs for calculating spectral irradiance from a radiative transfer model called “LibRadtran” were solar zenith angle (θ_z), aerosol optical depth (AOD), single scattering albedo (Society), asymmetry factor of aerosols, surface albedo, water vapor (W) and total ozone column (O_3). The AOD, SSA, asymmetry factor, surface albedo and W were derived from a sunphotometer (Cimel, model: CE318, see Figure 1(c)). This instrument is a part of AERONET (Aerosol RObotic NETwork) and the data are available on <https://aeronet.gsfc.nasa.gov/>. Total ozone column was retrieved from OMI/AURA satellite and the data is on the website: <https://avdc.gsfc.nasa.gov/pub/data/satellite/Aura/OMI/V03/L2OVP/>.

For the measured solar spectrum, a spectroradiometer (Instrument System, model: SP-320D, see Figure 1(d)) was used to collect spectral solar irradiance under overcast sky. The wavelength range of the measurements is 220-2400 nm, with the resolution of 1 nm in the wavelength range: 220-1700 nm and the resolution of 20 nm in the wavelength range: 1700-2400 nm.

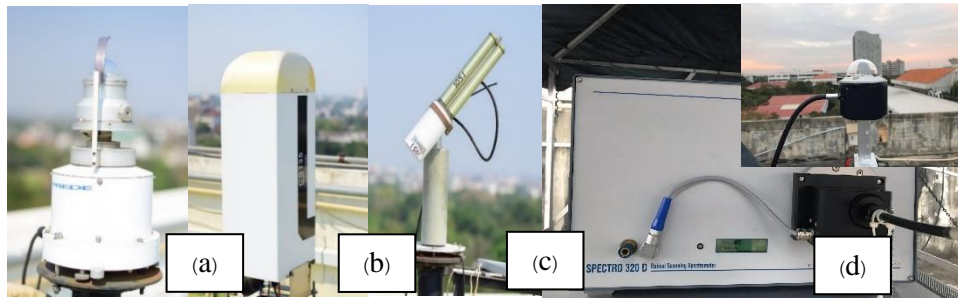


Figure 1. The instruments used in this work (a) sky view, (b) ceilometer, (c) sunphotometer and (d) spectroradiometer and probe

3. Methodology

The LibRadtran is a radiative transfer model used to estimate a spectral solar irradiance for entire spectrum from the wavelength of 120 nm to 100 μm . This model based on the DISORT (Discrete Ordinate Radiative Transfer) algorithm applying a plane parallel atmospheric assumption. In this study, we calculated spectral solar irradiance in the range of 300 to 2400 nm under overcast sky with a single layer of clouds and no rain. All inputs of LibRadtran consist of AOD, SSA, asymmetry factor, solar zenith angle, surface albedo, W , O_3 , CBH, effective radius and liquid water content of cloud. The sources of input data were shown in Table 1. These inputs were used in the LibRadtran and the result was the spectral solar irradiance in $\text{W}\cdot\text{m}^{-2}\cdot\text{nm}^{-1}$.

Afterwards, the spectral irradiance obtained from the LibRadtran was compared with that measured by the spectroradiometer. The difference between both dataset was presented in a statistical quantity of root mean square error (RMSE) expressed as follows:

Table 1. The source of parameters used to estimate spectral solar irradiance in LibRadtran

Input data	Source of data
Solar zenith angle	Calculation
AOD, SSA and Asymmetry factor	Sunphotometer
Surface albedo	Sunphotometer
W	Sunphotometer
O ₃	OMI/AURA Satellite
CBH	Ceilometer
Effective radius and Liquid water content	Literature [5,6]

$$\text{RMSE} = \sqrt{\frac{\sum_{i=1}^N (X_{\text{model},i} - X_{\text{meas},i})^2}{N}} \quad (\text{W} \cdot \text{m}^{-2} \cdot \text{nm}^{-1}) \quad (1)$$

where $X_{\text{model},i}$ is a spectral irradiance calculated from radiative transfer model ($\text{W} \cdot \text{m}^{-2} \cdot \text{nm}^{-1}$)

$X_{\text{meas},i}$ is a spectral irradiance measured from spectroradiometer ($\text{W} \cdot \text{m}^{-2} \cdot \text{nm}^{-1}$)

N is number of data

If the RMSE value approaches zero, it indicates that these two datasets are consistent.

4. Results and discussion

Examples of spectral solar irradiance collected by the spectroradiometer at 10.30 AM local time for three days in September 2019 were presented in Figure 2(a) and Figure 2(b) presented the spectral irradiance calculated from LibRadtran and that measured by the spectroradiometer on 2 September, 2019. From figure 2(a), the spectral solar irradiance on these days were different due to the cloud's layer and a path length of the sun. On 2 and 3 September, 2019, the skies were covered by a single layer cloud, whereas on 19 September, 2019, the multi-layer cloud, which attenuated more solar radiation than single layer clouds, were observed.

Figure 2(b) showed the comparison of the whole spectral solar irradiance from the LibRadtran and that from spectroradiometer on 2 September, 2019. The difference of the entire spectrum (not showed) was found in the range of -0.15 to $0.19 \text{ W}\cdot\text{m}^{-2}\cdot\text{nm}^{-1}$. The greatest difference occurred in a near infrared part (700-2400 nm), which was influentially affected by the water droplets inside the clouds.

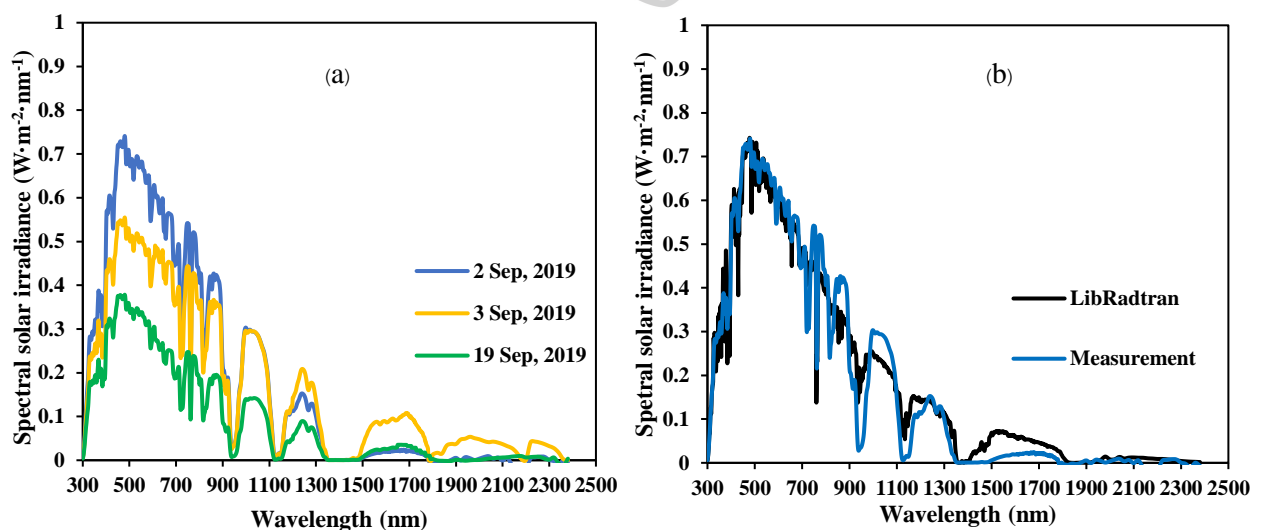


Figure 2. Examples of spectral solar irradiance under overcast sky from the spectroradiometer at 10.30 AM local time of different days in September 2019 (a) and the comparison of spectral solar irradiance from LibRadtran and spectroradiometer on 2 September, 2019 (b)

The comparison between the calculated and measured spectral solar irradiance under overcast sky for the period of August to December, 2019 was shown in Figure 3. The result showed that the spectral solar irradiance from both datasets were in reasonable agreement with the discrepancy in terms of RMSE of $0.043 \text{ W}\cdot\text{m}^{-2}\cdot\text{nm}^{-1}$. This difference of both data might cause from the variation of actual sky, which leads to the input properties of cloud. In the LibRadtran model, the sky was covered by only single homogeneous layer cloud and water droplet's properties (liquid water content, cloud effective radius) inside the clouds were set to be constant. Whereas, they might be a multi-layer cloud in the actual sky, which could reduce the spectral irradiance more than the LibRadtran model.

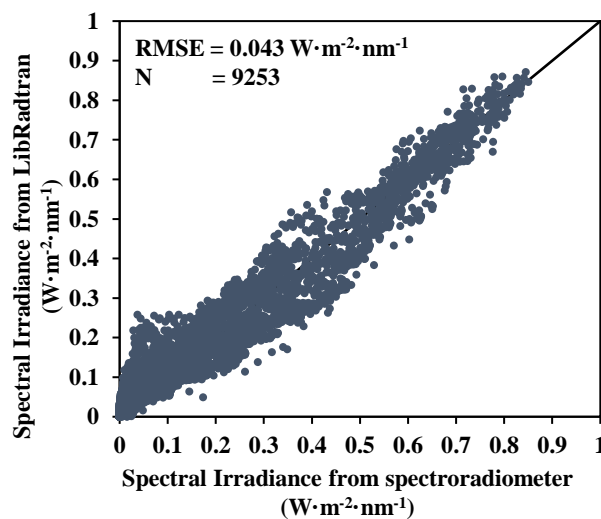


Figure 3. The comparison between spectral solar irradiance obtained from LibRadtran and that from the

5. Conclusion

In this work, the solar spectrums under overcast sky measured by the spectroradiometer were compared with those calculated from a radiative transfer model called “LIBRADTRAN” applying atmospheric parameters as its inputs during August – December 2019 at Nakhon Pathom, Thailand. It was found that the solar spectrum from the measurements and that from the calculation are in reasonable agreement, with the discrepancy in terms of RMSE of $0.043 \text{ W}\cdot\text{m}^{-2}\cdot\text{nm}^{-1}$. This comparing result indicates that this radiative transfer model is accurate enough for determining the optical properties of clouds which affect in surface solar radiation.

6. References

- [1] Page J 2012 The role of solar-radiation climatology in the design of photovoltaic systems *In Practical Handbook of Photovoltaics* (Academic Press) pp 573-643
- [2] Kasten F and Czeplak G 1980 Solar and terrestrial radiation dependent on the amount and type of cloud *Solar energy* pp 177-189
- [3] Matuszko D 2012 Influence of the extent and genera of cloud cover on solar radiation intensity *International Journal of Climatology* pp 2403-2414
- [4] Nann S and Riordan C 1991) Solar spectral irradiance under clear and cloudy skies: Measurements and a semiempirical model *Journal of Applied Meteorology* pp 447-462
- [5] Aufm-Kampe H J 1950 Visibility and liquid water content in clouds in the free atmosphere *Journal of meteorology* pp 54-57.
- [6] Nimnuan P Janjai S Nunez M Pratummasoot N Buntoung S Charuchittipan D Chanyatham T Chantraket P Tantiplubthong N 2017 Determination of effective droplet radius and optical depth of liquid water clouds over a tropical site in northern Thailand using passive microwave soundings, aircraft measurements and spectral irradiance data *Journal of Atmospheric and Solar-Terrestrial Physics* pp 8-18.



REFERENCES

- Aebi, C., Gröbner, J., Kazadzis, S., Vuilleumier, L., Gkikas, A., & Kämpfer, N. (2020). Estimation of cloud optical thickness, single scattering albedo and effective droplet radius using a shortwave radiative closure study in Payerne. *Atmospheric Measurement Techniques*, 13(2), 907-923.
- Ahrens, C. D. (2014). *Essentials of Meteorology : An Invitation to the Atmosphere 3rd edition* (3 ed.): Cengage Learning.
- Aufm Kampe, H. (1950). Visibility and liquid water content in clouds in the free atmosphere. *Journal of the Atmospheric Sciences*, 7(1), 54-57.
- Barnard, J. C., & Long, C. N. (2004). A simple empirical equation to calculate cloud optical thickness using shortwave broadband measurements. *Journal of Applied Meteorology*, 43(7), 1057-1066.
- Cano, D., Monget, J.-M., Albuisson, M., Guillard, H., Regas, N., & Wald, L. (1986). A method for the determination of the global solar radiation from meteorological satellite data. *Solar energy*, 37(1), 31-39.
- Cotton, W. R., & Anthes, R. A. (1992). *Storm and cloud dynamics*: Academic press.
- Ghonima, M., Urquhart, B., Chow, C., Shields, J., Cazorla, A., & Kleissl, J. (2012). A method for cloud detection and opacity classification based on ground based sky imagery. *Atmospheric Measurement Techniques*, 5(11), 2881-2892.
- Hess, M., Koepke, P., & Schult, I. (1998). Optical properties of aerosols and clouds: The software package OPAC. *Bulletin of the American meteorological society*, 79(5), 831-844.
- Huo, J., & Lu, D. (2009). Cloud determination of all-sky images under low-visibility conditions. *Journal of atmospheric and oceanic technology*, 26(10), 2172-2181.
- Iqbal, M. (2012). *An introduction to solar radiation*: Elsevier.
- Janjai, S., Wanvong, W., & Laksanaboonsong, J. (2006). *The determination of surface albedo of Thailand using satellite data*. Paper presented at the Proceedings of the 2nd Joint International Conference on Sustainable Energy and Environment (SEE'06).

- JMA. (2009). Conversion table of satellite data. from Japanese Meteorological Agency
- Lamb, D., & Verlinde, J. (2011). *Physics and chemistry of clouds*: Cambridge University Press.
- Leontieva, E., Stamnes, K., & Olseth, J. (1994). Cloud optical properties at Bergen (Norway) based on the analysis of long-term solar irradiance records. *Theoretical and applied climatology*, 50(1), 73-82.
- Liou, K.-N. (1992). Radiation and cloud processes in the atmosphere. Theory, observation, and modeling.
- Marshak, A., Knyazikhin, Y., Evans, K. D., & Wiscombe, W. J. (2004). The “RED versus NIR” plane to retrieve broken-cloud optical depth from ground-based measurements. *Journal of the Atmospheric Sciences*, 61(15), 1911-1925.
- Martinis, C., Wilson, J., Zablowski, P., Baumgardner, J., Aballay, J. L., Garcia, B., . . . Otero, L. (2013). A new method to estimate cloud cover fraction over El Leoncito Observatory from an all-sky imager designed for upper atmosphere studies. *Publications of the Astronomical Society of the Pacific*, 125(923), 56.
- Mayer, B., Kylling, A., Emde, C., Hamann, U., & Buras, R. (2012). libRadtran user’s guide. *Edition for libRadtran version, 1*.
- McFarquhar, G. M., & Heymsfield, A. J. (1998). The definition and significance of an effective radius for ice clouds. *Journal of the Atmospheric Sciences*, 55(11), 2039-2052.
- Meteorology, M. P. I. f. (2019, February 1, 2019). The climate system. Retrieved from <https://mpimet.mpg.de/en/communication/multimedia/figures/climate-system>
- Nakajima, T., & King, M. D. (1990). Determination of the optical thickness and effective particle radius of clouds from reflected solar radiation measurements. Part I: Theory. *Journal of Atmospheric Sciences*, 47(15), 1878-1893.
- Nakajima, T. Y., & Nakajima, T. (1995). Wide-area determination of cloud microphysical properties from NOAA AVHRR measurements for FIRE and ASTEX regions. *Journal of Atmospheric Sciences*, 52(23), 4043-4059.
- Nauss, T., & Kokhanovsky, A. A. (2011). Retrieval of warm cloud optical properties using simple approximations. *Remote Sensing of Environment*, 115(6), 1317-1325.
- NCAR, C. D. G. (2020). LIQUID WATER PATH: OVERVIEW. Retrieved from

<https://climatedataguide.ucar.edu/climate-data/liquid-water-path-overview>

- Nimnuan, P., Janjai, S., Nunez, M., Pratummasoot, N., Buntoung, S., Charuchittipan, D., Tantiplubthong, N. (2017). Determination of effective droplet radius and optical depth of liquid water clouds over a tropical site in northern Thailand using passive microwave soundings, aircraft measurements and spectral irradiance data. *Journal of Atmospheric and Solar-Terrestrial Physics*, 161, 8-18.
- Quante, M. (2004). *The role of clouds in the climate system*. Paper presented at the Journal de Physique IV (Proceedings).
- Ricchiazzi, P., Yang, S., & Gautier, C. (2000). SBDART: a practical tool for plane-parallel radiative transfer in the Earth's atmosphere. In.
- Serrano, D., Marín, M., Núñez, M., Utrillas, M., Gandía, S., & Martínez-Lozano, J. (2015). Wavelength dependence of the effective cloud optical depth. *Journal of Atmospheric and Solar-Terrestrial Physics*, 130, 14-22.
- Society, A. M. (2012, 20 February 2012). Liquid water path. Retrieved from https://glossary.ametsoc.org/wiki/Liquid_water_path
- Stephens, C. (1994). Remote sensing of the lower atmosphere, an introduction.
- Systems, R. S. (2022). Cloud Liquid Water Content. Retrieved from <https://www.remss.com/measurements/cloud-liquid-water-content/>
- Tohsing, K., Peengam, S., & Janjai, S. (2021). *Comparison of solar spectrum from measurements and that from radiative transfer model under overcast sky condition*. Paper presented at the Journal of Physics: Conference Series.
- Wilson, A., Scott, R., Cadeddu, M., Ghate, V., & Lubin, D. (2018). Cloud optical properties over West Antarctica from shortwave spectroradiometer measurements during AWARE. *Journal of Geophysical Research: Atmospheres*, 123(17), 9559-9570.
- Wolberg, J. (2006). *Data analysis using the method of least squares: extracting the most information from experiments*: Springer Science & Business Media.
- World Meteorological Organization, W. (1988). *Technical Regulations. Volume 1: General Meteorological Standards and Recommended Practices*.
- World Meteorological Organization, W. (2022). Classifying clouds. Retrieved from <https://public.wmo.int/en/WorldMetDay2017/classifying-clouds>

Wyser, K. (1998). The effective radius in ice clouds. *Journal of Climate*, 11(7), 1793-1802.





VITA

NAME Miss Sahussa Peengam

DATE OF BIRTH 10 September 1992

PLACE OF BIRTH Nakhon Pathom

INSTITUTIONS ATTENDED Silpakorn University

HOME ADDRESS 54/1 Moo 5 Samkwaipuek Sub-District, Mueang District,
Nakhon Pathom Province

PUBLICATION

1. Charuchittipan, D., Janjai, S., Pretummasoot, N., Buntoung, S., & Peengam, S. (2018). Mapping of cloud cover from satellite data over Thailand. *Science, Engineering and Health Studies*, 69-76.
2. Tohsing, K., Peengam, S., & Janjai, S. (2021). Comparison of solar spectrum from measurements and that from radiative transfer model under overcast sky condition. In *Journal of Physics: Conference Series* (Vol. 1719, No. 1, p. 012032). IOP Publishing.

